

# Dense Hebbian neural networks: a replica symmetric picture of supervised learning

---

**Elena Agliari,<sup>a</sup> Linda Albanese,<sup>b,f,g</sup> Francesco Alemanno,<sup>b,f</sup> Andrea Alessandrelli,<sup>c</sup> Adriano Barra,<sup>b,f</sup> Fosca Giannotti,<sup>d,e</sup> Daniele Lotito,<sup>c,f</sup> Dino Pedreschi,<sup>c</sup>**

<sup>a</sup>*Dipartimento di Matematica, Sapienza Università di Roma, Piazzale Aldo Moro, 5, 00185, Roma, Italy*

<sup>b</sup>*Dipartimento di Matematica e Fisica, Università del Salento, Via per Arnesano, 73100, Lecce, Italy*

<sup>c</sup>*Dipartimento di Informatica, Università di Pisa, Lungarno Antonio Pacinotti, 43, 56126, Pisa, Italy*

<sup>d</sup>*Scuola Normale Superiore, Piazza dei Cavalieri 7, 56126, Pisa, Italy*

<sup>e</sup>*Istituto di Scienza e Tecnologie dell' Informazione, Via Giuseppe Moruzzi, 1, 56124 Pisa, Italy*

<sup>f</sup>*Istituto Nazionale di Fisica Nucleare, Campus Ecotekne, Via Monteroni, 73100, Lecce, Italy*

<sup>g</sup>*Scuola Superiore ISUFI, Campus Ecotekne, Via Monteroni, 73100, Lecce, Italy*

**ABSTRACT:** We consider dense, associative neural-networks trained by a teacher (i.e., with supervision) and we investigate their computational capabilities analytically, via statistical-mechanics of spin glasses, and numerically, via Monte Carlo simulations. In particular, we obtain a phase diagram summarizing their performance as a function of the control parameters such as quality & quantity of the training dataset, network storage and noise, that is valid in the limit of large network size and structureless datasets: these networks may work in a ultra-storage regime (where they can handle a huge amount of patterns, if compared with shallow neural networks) or in a ultra-detection regime (where they can perform pattern recognition at prohibitive signal-to-noise ratios, if compared with shallow neural networks). Guided by the random theory as a reference framework, we also test numerically learning, storing and retrieval capabilities shown by these networks on structured datasets as MNist and Fashion MNist. As technical remarks, from the analytic side, we implement large deviations and stability analysis within Guerra's interpolation to tackle the not-Gaussian distributions involved in the post-synaptic potentials while, from the computational counterpart, we insert Plefka approximation in the Monte Carlo scheme, to speed up the evaluation of the synaptic tensors, overall obtaining a novel and broad approach to investigate supervised learning in neural networks, beyond the shallow limit, in general.

---

## Contents

<b>1</b>	<b>Introduction</b>	<b>1</b>
<b>2</b>	<b>Dense Hebbian Neural Network in the supervised setting</b>	<b>3</b>
<b>3</b>	<b>Analytical findings</b>	<b>6</b>
3.1	Ultra-storage capacity limit	10
3.2	Ultra-noise tolerance limit	10
3.3	Low entropy datasets	11
<b>4</b>	<b>Numerical findings</b>	<b>13</b>
4.1	Stability analysis and Monte Carlo simulations	13
4.2	Application to structured dataset	17
4.3	Comparison between unsupervised and supervised regime	23
<b>5</b>	<b>Conclusion and outlooks</b>	<b>25</b>
<b>A</b>	<b>Large Deviations Theory's computation</b>	<b>26</b>
<b>B</b>	<b>Proof of Proposition 1</b>	<b>28</b>
<b>C</b>	<b>Evaluation of momenta of the effective post-synaptic potential</b>	<b>32</b>
<b>D</b>	<b>Plefka's Expansion on Gibbs potential</b>	<b>33</b>

---

## 1 Introduction

The research covered by this paper, coupled to its twin work [1] addressing the unsupervised counterpart, aims to provide an exhaustive picture of (supervised) Hebbian learning by dense networks (namely networks whose neural dialogues happen in assemblies of  $P > 2$  interacting units rather than in standard neural couples, i.e.  $P = 2$ ), inspecting their emerging computational capabilities by means of statistical mechanics of disordered systems [7, 13, 37, 45]. In these regards, statistical mechanical investigations on dense spin glasses [6, 15, 16, 23, 26, 33, 48, 52] constitutes by a long time a fertile ground where these novel Hebbian theories on dense neural networks can germinate. Indeed, in the past, statistical mechanics already played a pivotal role for describing and quantifying information processing by neural networks for shallow (see e.g. [5, 14, 27, 30, 38]), deep (see e.g., [2, 11, 17, 36, 47]) and dense (see e.g. [4, 9, 19, 39, 41]) architectures: the ultimate reward we obtain by this approach lies in the knowledge of *phase diagrams*, namely plots in the space of the network's control parameters (e.g., network size and connectivity, storage load, noise, dataset quality and quantity, etc.) where different emerging computational capabilities (e.g. learning, storage, recognition, associativity, denoising, etc.) are related to particular regions in these diagrams much as the phase diagram of the water summarizes effectively in a plot with solely three control parameters (i.e., pressure, volume and temperature) the

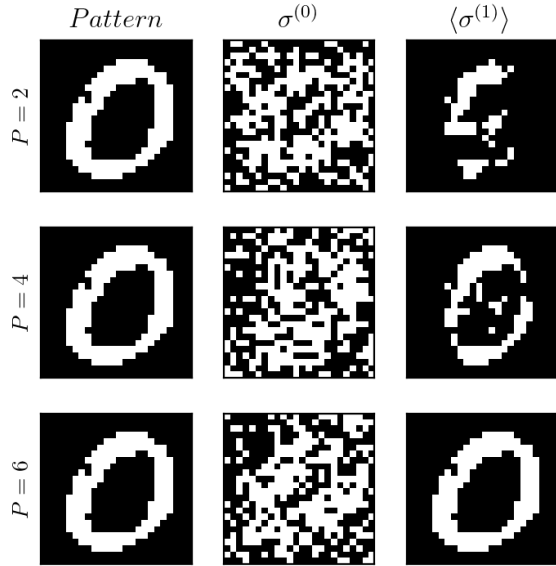


**Figure 1:** Example of a reconstruction of a pattern at a very low signal-to-noise ratio: we select an example of a pattern, a 0 from the MNist dataset (first column), and we add it further noise by flipping randomly  $\sim 50\%$  of its pixels (second column): this image constitutes the input  $\sigma^{(0)}$  that the networks experience. In particular, three networks are used,  $P = 2$  (first line) that is the standard Hopfield model,  $P = 4$  (second line) and  $P = 6$  (third line). In all the three lines, in the third column we report reconstructions  $\langle \sigma^{(1)} \rangle$  (achieved by a single MC step equipped with Plefka’s dynamics [49], *vide infra*): with a grade of interaction  $P = 6$  the network manages to perfectly retrieve the zero, while networks with less dense interactions fail.

different *regimes* (e.g. vapor, liquid, solid) in which a network of water molecules can be found. Much as these regions are split by phase transitions in Physics, “computational phase transitions” delimit -in the phase diagram- the various working regions of neural networks [28, 43, 46]: it is our credo that the knowledge of phase diagrams, with their related computational phase transitions, for the various modern neural architectures can be helpful in the field of Sustainable AI (SAI) and Optimized AI (OAI) as this allows preparing the network in an optimal setting for a given task, with thus possible energy saving (e.g., by avoiding training when it is theoretically forbidden). Further, the mathematical control that results by statistical mechanical treatments of neural networks suggests that such a discipline may constitute a main strand also toward eXplainable AI (XAI).

Since the first wave of statistical mechanical formalization in the late eighties and early nineties of the past century, how these networks accomplish learning was a central question -addressed from various perspectives (see e.g. [30, 32, 51, 55])- yet solely “storing” was studied at that time, in the dense network scenario [18, 24, 31]: in this simpler limit, the network experiences just once the patterns to cope with and stores them in its Hebbian synaptic tensor for suitable successive pattern recognition usage but it does not undergo a real “learning process”, where the network does not have access to the patterns to store rather it has to form its own representation of them just by experiencing their noisy examples provided in form of datasets to analyze: here we deepen this phenomenon moving from Hebbian storing to supervised Hebbain learning (and referring to [1] for its unsupervised counterpart).

We stress that while, from a biological modeling perspective, these dense networks lack to find a crystal clear inspiration (as neurons interact mainly in couples, despite higher order generalizations can still be seen as abstract effective models [40]), in Machine Learning there are no restrictions preventing their usage, thus prompting the present investigation where we prove that there can be manifest rewards in the usage of networks with broad interactions w.r.t. the standard pairwise case. Dense networks may indeed be used in two different operational modes, both forbidden to shallow machines, (i) a ultra-storage regime (that extends the high-load regime of the standard Hopfield model to the dense case), where these networks handle a by far larger number of patterns w.r.t. the standard  $P = 2$  limit and (ii) a ultra-tolerance regime (that extends the low-load of the standard Hopfield model to the dense case) where these networks perform pattern recognition at prohibitive signal-to-noise ratio w.r.t. the  $P = 2$  limit. Clearly these capabilities have a cost, indeed -as we will quantify along the paper- the main flaw in the usage of dense networks is that they require large volumes of training examples (far beyond the  $P = 2$  limit) and thus energy consumption, however -at difference with the unsupervised case [1]- when learning with a teacher, the cost for training is always the same, no matter if the assemblies happen for  $P = 6$  or -say-  $P = 60$ : the independence by  $P$  of the thresholds for learning is a crucial new finding we prove in this paper and it strongly suggests the usage of dense networks when dealing with several extremely-noisy patterns and no large datasets are available: see Figure 1 to appreciate the concrete usefulness of working with a dense setting (compared to the standard pairwise case).

The theory we work out here deals with networks learning from random datasets, where everything can be treated analytically (at the replica symmetric level of description) and it is successfully tested against Monte Carlo simulations and further corroborated on structured datasets (MNist and Fashion-MNist), where numerical results returned overall a very good qualitative agreement with theoretical predictions.

Technically speaking, analytically we solve for the statistical mechanics of these networks by adapting the Guerra's interpolation technique (see e.g. [4, 21, 22]): this result in a non-trivial generalization because, as interactions are dense and thus fluctuations in the post-synaptic potentials no longer Gaussian, we can not assume the universality property of the quenched noise in spin glasses to hold and we need to evaluate the lower order momenta of the distributions of these potentials -that enter in the calculations of the Guerra scheme- by relying on alternative approaches. In particular we mix large deviation theory (to bound their values) with stability analysis (to estimate them). At the numerical level, as the update of dense synaptic tensor results is a bottleneck for any dynamical update rule, we implement the Plefka effective scheme [49] to speed up this evaluation thus obtaining overall a new approach for tackling the statistical mechanics of neural networks with complex architectures in broad generality.

## 2 Dense Hebbian Neural Network in the supervised setting

In this section we describe dense associative neural networks, namely Hebbian networks with a *density* (i.e. a grade of interaction  $P$  among neurons) greater than  $P = 2$  trained in a supervised regime. We start addressing them via statistical mechanics: the ultimate purpose of this approach is to work out phase diagrams splitting the space of the control parameters (e.g. storage, density, noise and dataset size) into regions where the network shows different emerging computational capabilities. To reach this goal we need to introduce control and order parameters for the present case and express the (quenched) statistical pressure -or free energy, i.e. the main observable in statistical mechanics [45]- in terms of these parameters. Finally, by extremizing the statistical pressure w.r.t. the order parameters

we obtain a set of self-consistent equations for the evolution of these order parameters in the space of the control parameters, whose investigation ultimately provides the phase diagrams of these networks. As technical remark we stress that we work under the standard replica symmetric assumption (namely we assume that all the order parameters self-average around their means in the asymptotic limit). Dense associative neural networks are Hopfield models with  $P$ -order interactions, studied here as endowed with supervised Hebbian couplings. More precisely, in this system  $N$  binary neurons  $\sigma = (\sigma_1, \sigma_2, \dots, \sigma_N) \in \{-1, +1\}^N$  interact in groups of  $P$  spins and the classical Hebb's rule is revised in such a way that it is built over a set of perturbed version of some unknown archetypes and meant as a result of a supervised learning. The  $K$  Rademacher archetypes that the network has to infer, store and eventually retrieve, are defined as  $\{\xi^\mu\}_{\mu=1,\dots,K}$  with

$$\mathbb{P}(\xi_i^\mu) = \frac{1}{2} \left[ \delta_{\xi_i^\mu, -1} + \delta_{\xi_i^\mu, +1} \right] \quad (2.1)$$

for  $i = 1, \dots, N$  and  $\mu = 1, \dots, K$ , and we introduce  $M$  examples (per archetype) -denoted as  $\{\eta^{\mu,a}\}_{a=1,\dots,M}^{\mu=1,\dots,K}$  with  $\eta^{\mu,a} \in \{-1, +1\}^N$ - as perturbed versions of the archetypes, as

$$\eta_i^{\mu,a} = \xi_i^\mu \cdot \chi_i^{\mu,a}, \quad (2.2)$$

where  $\chi_i^{\mu,a}$  is a Bernoullian random variable, namely

$$\mathbb{P}(\chi_i^{\mu,a}) = \frac{1+r}{2} \delta_{\chi_i^{\mu,a}, +1} + \frac{1-r}{2} \delta_{\chi_i^{\mu,a}, -1}, \quad (2.3)$$

where  $r \in (0, 1)$  for  $i = 1, \dots, N$  and  $\mu = 1, \dots, K$ . Notice that  $r$  plays as a dataset-quality parameter: as  $r \rightarrow 1$  examples collapse on the related archetypes, while as  $r \rightarrow 0$  examples turn out to be uncorrelated with the related archetypes.

The network is supplied with the dataset  $\{\eta^{\mu,a}\}_{a=1,\dots,M}^{\mu=1,\dots,K}$  and it is asked to reconstruct the unknown archetypes  $\{\xi^\mu\}_{\mu=1,\dots,K}$ . The available information is allocated in the interaction strength among neurons (i.e. the Hebbian synaptic tensors  $J_{i_1, \dots, i_P}^{sup}$  as defined by eq. (2.10), *vide infra*), as specified by the following

**Definition 1.** *The cost function (or Hamiltonian) of the dense Hebbian neural network in the supervised regime is*

$$\mathcal{H}_{N,K,M,r}^{(P)}(\sigma|\xi, \chi) = - \frac{N}{P! \mathcal{R}^{P/2}} \sum_{\mu=1}^K \left( \frac{1}{NM} \sum_{i=1}^N \sum_{a=1}^M \xi_i^\mu \chi_i^{\mu,a} \sigma_i \right)^P \quad (2.4)$$

where  $P$  is the interaction order (assumed as even) and we pose  $\mathcal{R} := r^2 + \frac{1-r^2}{M}$ .

Once introduced the noise  $\beta \in \mathcal{R}^{+1}$  (such that for  $\beta \rightarrow 0$  neural dynamics is a pure uncorrelated random walk while for  $\beta \rightarrow \infty$  it is a steepest descent toward the minima of the Cost function, the latter playing as the Lyapunov function in this case), the related partition function of the model is defined as

$$\mathcal{Z}_{N,K,M,\beta,r}^{(P)}(\xi, \chi) = \sum_{\sigma} \exp \left( -\beta \mathcal{H}_{N,K,M,r}^{(P)}(\sigma|\xi, \chi) \right) =: \sum_{\sigma} \mathcal{B}_{N,K,M,\beta,r}^{(P)}(\sigma|\xi, \chi) \quad (2.5)$$

where  $\mathcal{B}_{N,K,M,\beta}^{(P)}(\sigma|\xi, \chi)$  is denoted as Boltzmann factor.

---

<sup>1</sup>Note that, in Physics, in proper units  $\beta = 1/T$ ,  $T$  is the temperature.

At finite network size  $N$ , the quenched pressure of this model reads as

$$\mathcal{A}_{N,K,M,\beta,r}^{(P)} = \frac{1}{N} \mathbb{E} \log \mathcal{Z}_{N,K,M,\beta,r}^{(P)}(\boldsymbol{\xi}, \boldsymbol{\chi}) \quad (2.6)$$

where  $\mathbb{E} = \mathbb{E}_{\chi} \mathbb{E}_{\xi}$  denotes the average over the realization of examples, namely over the distributions (2.1) and (2.3).

By combining the quenched average  $\mathbb{E}[\cdot]$  and the Boltzmann average

$$\omega[\cdot] := \frac{1}{\mathcal{Z}_{N,K,M,\beta,r}^{(P)}(\boldsymbol{\xi}, \boldsymbol{\chi})} \sum_{\boldsymbol{\sigma}}^{2^N} \cdot \mathcal{B}_{N,K,M,\beta,r}^{(P)}(\boldsymbol{\sigma} | \boldsymbol{\xi}, \boldsymbol{\chi}), \quad (2.7)$$

possibly replicated over to two or more replicas<sup>2</sup>, that is,  $\Omega(\cdot) := \omega(\cdot) \times \omega(\cdot) \dots \times \omega(\cdot)$ , we get the expectation

$$\langle \cdot \rangle := \mathbb{E} \Omega(\cdot). \quad (2.8)$$

We stress that, expanding the Hamiltonian in (2.4), we get

$$\mathcal{H}_{N,K,M,r}^{(P)}(\boldsymbol{\sigma} | \boldsymbol{\xi}, \boldsymbol{\chi}) = - \frac{1}{P! \mathcal{R}^{P/2} M^P N^{P-1}} \sum_{\mu=1}^K \sum_{i_1, \dots, i_P}^{N, \dots, N} \sum_{a_1, \dots, a_P}^{M, \dots, M} \xi_{i_1}^{\mu} \chi_{i_1}^{\mu, a_1} \dots \xi_{i_P}^{\mu} \chi_{i_P}^{\mu, a_P} \sigma_{i_1} \dots \sigma_{i_P} + \mathcal{O}(KN^{1-P/2}); \quad (2.9)$$

in this way we can highlight the generalization of the interaction matrix in supervised regime for  $P \geq 2$  which is

$$J_{i_1 \dots i_P}^{(sup)} = \frac{1}{\mathcal{R}^{P/2} M^P} \sum_{\mu=1}^K \sum_{a_1, \dots, a_P}^{M, \dots, M} \xi_{i_1}^{\mu} \chi_{i_1}^{\mu, a_1} \dots \xi_{i_P}^{\mu} \chi_{i_P}^{\mu, a_P}. \quad (2.10)$$

Note that in Sec. 4.3 we compare outcomes of these networks trained under supervised learning vs. those stemming by the same networks but trained with no supervision (the theory for unsupervised learning by dense networks appeared in a mirror paper [1]): ultimately the key role of the teacher in Hebbian learning -resembling classical supervision in Machine Learning- consists in grouping together all the examples pertaining to the same archetype before presenting them to the network (while such ordering is not available in the unsupervised scheme).

We introduce the storage (or load)  $\alpha_b$  the network has to face as specified by the following

**Definition 2.** In the thermodynamic limit  $N \rightarrow \infty$ , the network storage -or load- is defined as

$$\lim_{N \rightarrow +\infty} \frac{K}{N^b} =: \alpha_b < \infty \quad (2.11)$$

with  $b \leq P - 1$ .<sup>3</sup> Further, the statistical pressure in the thermodynamic limit is denoted as

$$\mathcal{A}_{\beta, r, \alpha_b}^{(P)} = \lim_{N \rightarrow \infty} \mathcal{A}_{N, K, M, \beta, r}^{(P)}. \quad (2.12)$$

In the next Section, we will see that -much as we can split the analysis of the shallow Hopfield model in *low storage* and *high storage* cases- also in this dense counterpart we can study network's behavior in two rather different operational regimes: a regime of saturation, called *ultra-storage capacity* and

<sup>2</sup>A replica is an independent copy of the system characterized by the same realization of disorder, namely by the same realization of the archetypes and examples and, thus, of the synaptic tensors.

<sup>3</sup>The case  $b > P - 1$  is known to lead to a black-out scenario [18, 24] not useful for computational purposes and shall be neglected here.

afforded in Sec. 3.1- where the network can infer, store and retrieve up to  $K \propto N^{P-1}$  archetypes (hence achieved by fixing  $b = P - 1$  in the network's load above); and a regime away from saturation, called *ultra-noise tolerance* -deepened in Sec. 3.2- where the network can detect signals i.e., it can infer archetypes behind the provided examples, even if the latter are extremely noisy (namely working at signal-to-noise ratios forbidden to shallow networks): this setting is achieved by requiring  $b < P - 1$  in the network's load above.

We need to introduce now a set of observables, known as *order parameters* of the theory, which are for  $\mu = 1, \dots, K$

$$\begin{aligned} n_\mu &= \frac{r}{\mathcal{R}} \frac{1}{NM} \sum_{i,a=1}^{N,M} \eta_i^{\mu,a} \sigma_i, \\ m_\mu &= \frac{1}{N} \sum_{i=1}^N \xi_i^\mu \sigma_i, \\ q_{ab} &= \frac{1}{N} \sum_{i=1}^N \sigma_i^{(a)} \sigma_i^{(b)}, \end{aligned} \tag{2.13}$$

where  $a$  and  $b$  are two replicas.

We stress that  $m_\mu$  quantifies the alignment of the network configuration  $\sigma$  with the archetype  $\xi^\mu$ ,  $n_\mu$  compares the alignment of the network configuration with the average of all the examples labeled by  $\mu$  (i.e. pertaining to the  $\mu^{th}$  archetype) and  $q_{ab}$  is the standard two-replica overlap between the replicas  $\sigma^{(a)}$  and  $\sigma^{(b)}$ .

### 3 Analytical findings

In this section we solve -through Replica-Symmetric assumption- the statistical mechanics of dense Hebbian neural network in supervised regime, namely we obtain the explicit expression of its quenched statistical pressure in terms of control and order parameters (in the thermodynamic limit) and we extremize it to obtain the set of self-consistency equations, whose solutions trace the evolution of the order parameters in the space of the control parameters ultimately allowing to draw the phase diagram related to these networks under this learning protocol.

To do so, we exploit Guerra's interpolation technique [35], yet some adjustments to face the non-gaussianity nature of quenched noise in dense networks are in order this time and, mirroring the procedure performed in [1], we enrich the Guerra's interpolation technique with large deviation theory and stability analysis (to supply to the lack of universality properties of quenched noises in dense spin glasses).

Before proceeding, we recall that, as standard (see e.g. [27]) and with no loss of generality, in the following we will focus on the ability of the network to learn and retrieve the first archetype  $\xi^1$ . Thus, in the next expression, the contribution corresponding to  $\mu = 1$  shall be split from all the others and interpreted as the *signal* contribution, while the remaining ones (i.e. those with  $\mu \neq 1$ ) make up the slow-noise contribution impairing both learning and retrieval of  $\xi^1$ .

Starting from the partition function in Equation (2.5), we handle it in order to have an integral representation which allows us a convenient form for interpolation technique. Starting from Eq. (2.5),

we apply the functional generator<sup>4</sup> and the Hubbard-Stratonovich transformation to get,

$$\begin{aligned}
\mathcal{Z}_{N,K,\rho,\beta}^{(P)}(\boldsymbol{\xi}, \boldsymbol{\chi}) &= \lim_{J \rightarrow 0} \mathcal{Z}_{N,K,M,\beta}^{(P)}(\boldsymbol{\xi}, \boldsymbol{\chi}; J) \\
&= \lim_{J \rightarrow 0} \sum_{\boldsymbol{\sigma}} \int \prod_{\mu} d\mu(z_{\mu}) \exp \left[ J \sum_i \xi_i^1 \sigma_i + \beta' \frac{N}{2} (1 + \rho)^{P/2} n_1^P(\boldsymbol{\sigma}) \right. \\
&\quad \left. + \sqrt{\frac{\beta'}{N^{P-1} \mathcal{R}^{P/2}}} \sum_{\mu > 1}^K \sum_{i_1, \dots, i_{P/2}}^{N, \dots, N} \left( \frac{1}{M^{P/2}} \sum_{a_1, \dots, a_{P/2}}^{M, \dots, M} \xi_{i_1}^{\mu} \chi_{i_1}^{\mu, a_1} \dots \xi_{i_{P/2}}^{\mu} \chi_{i_{P/2}}^{\mu, a_{P/2}} \right) \sigma_{i_1} \dots \sigma_{i_{P/2}} z_{\mu} \right] \tag{3.1}
\end{aligned}$$

where  $\rho := \frac{1 - r^2}{r^2 M}$ ,  $\beta' := 2\beta/P!$  and  $d\mu(z_{\mu}) = \frac{dz_{\mu}}{\sqrt{2\pi}} \exp\left(-\frac{z_{\mu}^2}{2}\right)$  corresponds to Gaussian measure.

**Remark 1.** *Pivotal for numerical implementation, note that we can think at the above transformation as a mapping between the original dense Hebbian network and a restricted Boltzmann machine where  $K$  hidden neurons  $z_{\mu}$  (equipped with a Gaussian prior) interact with the  $N$  visible neurons  $\sigma$  grouped in  $\sigma_{i_1} \dots \sigma_{i_{P/2}}$ <sup>5</sup>. Note further that, in this integral representation of the partition function there is a one-to-one correspondence among the number of patterns to store ( $K$ ) and the amount of hidden neurons ( $K$ ), suggesting to allocate one hidden neuron to the recognition of a specific pattern: this setting is historically known as grandmother cell [12, 34].*

In the following we refer to  $\rho$  as *dataset entropy*: strictly speaking,  $\rho$  is not entropy, yet here we allow ourselves for this slight abuse of language because, as discussed in [12] for the case of pair-wise interactions, the conditional entropy  $H(\boldsymbol{\xi}^{\mu} | \boldsymbol{\eta}^{\mu, a})$ , that quantifies the amount of information needed to describe the original message  $\boldsymbol{\xi}^{\mu}$  given the  $M$  examples  $\boldsymbol{\eta}^{\mu, a}$ , is a monotonically increasing function of  $\rho$ .

Using the CLT on the variable  $\frac{1}{M} \sum_a^M \xi_i^{\mu} \chi_i^{\mu, a}$ , we can replace each contributions in the noise term in the brackets with  $\sqrt{\mathcal{R}} \phi_i^{\mu}$  with  $\phi_i^{\mu} \sim \mathcal{N}(0, 1)$ , thus we get

$$\begin{aligned}
\mathcal{Z}_{N,K,\rho,\beta}^{(P)}(\boldsymbol{\xi}, \boldsymbol{\chi}) &= \lim_{J \rightarrow 0} \mathcal{Z}_{N,K,M,\beta,r}^{(P)}(\boldsymbol{\xi}, \boldsymbol{\chi}; J) \\
&= \lim_{J \rightarrow 0} \sum_{\boldsymbol{\sigma}} \int \prod_{\mu} d\mu(z_{\mu}) \exp \left[ J \sum_i \xi_i^1 \sigma_i + \beta' \frac{N}{2} (1 + \rho)^{P/2} n_1^P(\boldsymbol{\sigma}) \right. \\
&\quad \left. + \sqrt{\frac{\beta'}{N^{P-1}}} \sum_{\mu > 1}^K \sum_{i_1, \dots, i_{P/2}}^{N, \dots, N} \left( \phi_{i_1}^{\mu} \dots \phi_{i_{P/2}}^{\mu} \right) \sigma_{i_1} \dots \sigma_{i_{P/2}} z_{\mu} \right] \tag{3.2}
\end{aligned}$$

If we focus on the noise term and, in particular, on the random variable in the brackets, using large deviations theory we can approximate it with a Gaussian random variable  $\lambda_{i_1, \dots, i_{P/2}}^{\mu}$  with zero mean and  $\sqrt{\mathcal{V}}$  standard deviation, where  $\mathcal{V}$  has to be evaluated later on (by relying upon stability analysis and large deviation theory, as explained in Section 4.1 and deepened in Appendix A).

<sup>4</sup>We add the term  $J \sum_i \xi_i^1 \sigma_i$  in the exponent of the Boltzmann factor to generate the expectations of the Mattis magnetization  $m_1$ . To do so, we evaluate the derivative w.r.t.  $J$  of the quenched statistical pressure at  $J = 0$ .

<sup>5</sup>This equivalence holds also for the pairwise Hopfield model [20] and higher order-Boltzmann machines [3, 50].

Therefore, we have reached an effective integral representation for supervised dense Hebbian neural networks that reads as

$$\begin{aligned} \mathcal{Z}_{N,K,\rho,\beta}^{(P)}(\boldsymbol{\xi}, \boldsymbol{\chi}) &= \lim_{J \rightarrow 0} \mathcal{Z}_{N,K,M,\beta,r}^{(P)}(\boldsymbol{\xi}, \boldsymbol{\chi}; J) \\ &= \lim_{J \rightarrow 0} \sum_{\boldsymbol{\sigma}} \int \prod_{\mu} d\mu(z_{\mu}) \exp \left[ J \sum_i \xi_i^1 \sigma_i + \beta' \frac{N}{2} (1 + \rho)^{P/2} n_1^P(\boldsymbol{\sigma}) \right. \\ &\quad \left. + \sqrt{\frac{\beta' \mathcal{V}}{N^{P-1}}} \sum_{\mu > 1}^K \sum_{i_1, \dots, i_{P/2}}^{N, \dots, N} \lambda_{i_1, \dots, i_{P/2}}^{\mu} \sigma_{i_1} \dots \sigma_{i_{P/2}} z_{\mu} - \frac{\beta'}{2} K \mathcal{V} N^{1-P/2} \right] \end{aligned} \quad (3.3)$$

where  $\lambda_{i_1, \dots, i_{P/2}}^{\mu}$  are the aforementioned Gaussian i.i.d. variables and the last term represents the subtraction of the diagonal term. To keep the reading more fluent, we anticipate (see eq. (4.19)) that

$$\mathcal{V} = \sqrt{\frac{P(2P-3)!!}{2}}. \quad (3.4)$$

Now we want to find the self-consistency relations for the order parameters introduced in equations (2.13) by generalizing a Guerra's interpolating technique [21]. The underlying idea behind the original technique is to introduce a generalized statistical pressure that interpolates between the original model (which is the target of our investigation but we are not able to address it directly) and a simple one (which is usually a one-body model that we can solve exactly). We thus find the solution of the latter and thus propagate the obtained solution back to the original model by the fundamental theorem of calculus.

In this last passage we assume the replica symmetry (*vide infra*), namely, we assume that the order-parameter fluctuations are negligible in the thermodynamic limit: this property makes the integral in the fundamental theorem of calculus analytical. Let us start with some definitions.

**Definition 3.** *Given the interpolating parameter  $t \in [0, 1]$ , the real-valued constants  $A, B, C, \psi$  (whose specific values are to be set a posteriori) and i.i.d. standard Gaussian variables  $Y_i, J_{\mu} \sim \mathcal{N}(0, 1)$  for  $i = 1, \dots, N$ ,  $\mu = 1, \dots, K$ , the interpolating partition function is given as*

$$\begin{aligned} \mathcal{Z}_{N,K,\rho,\beta}^{(P)}(\boldsymbol{\xi}, \boldsymbol{\chi}; J, t) &= \sum_{\{\boldsymbol{\sigma}\}} \int d\mu(z_{\mu}) \exp \left[ J \sum_i \xi_i^1 \sigma_i + t \beta' \frac{N}{2} (1 + \rho)^{P/2} n_1^P(\boldsymbol{\sigma}) \right. \\ &\quad \left. + \sqrt{t} \sqrt{\frac{\beta' \mathcal{V}}{N^{P-1}}} \sum_{\mu > 1}^K \sum_{i_1, \dots, i_{P/2}}^{N, \dots, N} \lambda_{i_1, \dots, i_{P/2}}^{\mu} \sigma_{i_1} \dots \sigma_{i_{P/2}} z_{\mu} + \frac{1-t}{2} C \sum_{\mu > 1}^K z_{\mu}^2 \right. \\ &\quad \left. + (1-t) \frac{N}{2} \psi n_1(\boldsymbol{\sigma}) + \sqrt{1-t} \left( A \sum_{i=1}^N Y_i \sigma_i + B \sum_{\mu > 1}^K \tilde{J}_{\mu} z_{\mu} \right) - \frac{\beta'}{2} \mathcal{V} K N^{P/2} \right]. \end{aligned} \quad (3.5)$$

**Remark 2.** *The interpolating partition function  $\mathcal{Z}_{N,K,\rho,\beta}^{(P)}(\boldsymbol{\xi}, \boldsymbol{\chi}; J, t)$  is determined in such a way that when  $t = 1$  we recover the original model (2.5) and for  $t = 0$  we recover a model simple enough to be solved directly.*

Mirroring [1], we introduce an interpolating quenched statistical pressure that reads as

**Definition 4.** The interpolating statistical pressure related to the partition function (3.5) is introduced as

$$\mathcal{A}_{N,K,\rho,\beta}^{(P)}(t) := \frac{1}{N} \mathbb{E} \left[ \ln \mathcal{Z}_{N,K,\rho,\beta}^{(P)}(\boldsymbol{\xi}, \boldsymbol{\chi}; J, t) \right], \quad (3.6)$$

where the expectation  $\mathbb{E}$  is now meant over  $\lambda_{i_1, \dots, i_{P/2}}^\mu$ ,  $\{Y_i\}_{i=1, \dots, N}$ , and  $\{J_{\mu,a}\}_{\mu=1, \dots, K}^{a=1, \dots, M}$  too.

In the thermodynamic limit,

$$\mathcal{A}_{\rho,\beta,\alpha_b}^{(P)}(t) := \lim_{N \rightarrow \infty} \mathcal{A}_{N,K,\rho,\beta}^{(P)}(t). \quad (3.7)$$

By setting  $t = 1$  the interpolating pressure recovers the original one (2.6), that is  $\mathcal{A}_{N,K,\rho,\beta,\alpha_b}^{(P)} = \mathcal{A}_{N,K,\rho,\beta,\alpha_b}^{(P)}(t = 1)$ .

The interpolation for the statistical pressure implies an interpolating measure, whose related Boltzmann factor reads as

$$\begin{aligned} \mathcal{B}_{N,K,\rho,\beta}^{(P)}(\boldsymbol{\sigma} | \boldsymbol{\xi}, \boldsymbol{\chi}; J, t) := & \exp \left[ J \sum_i \xi_i^1 \sigma_i + t \beta' \frac{N}{2} (1 + \rho)^{P/2} n_1^P(\boldsymbol{\sigma}) + (1 - t) \frac{N}{2} \psi n_1(\boldsymbol{\sigma}) \right. \\ & + \sqrt{t} \sqrt{\frac{\beta' \mathcal{V}}{N^{P-1}}} \sum_{\mu > 1}^K \sum_{i_1, \dots, i_{P/2}}^{N, \dots, N} \lambda_{i_1, \dots, i_{P/2}}^\mu \sigma_{i_1} \cdots \sigma_{i_{P/2}} z_\mu + \frac{\beta'}{2} K N^{P/2} \\ & \left. + \sqrt{1-t} \left( A \sum_{i=1}^N Y_i \sigma_i + B \sum_{\mu > 1}^K \tilde{J}_\mu z_\mu \right) + \frac{1-t}{2} C \sum_{\mu > 1}^K z_\mu^2 \right], \end{aligned} \quad (3.8)$$

by which the partition function can be written as

$$\mathcal{Z}_{N,K,\rho,\beta}^{(P)}(\boldsymbol{\xi}, \boldsymbol{\chi}; J, t) = \sum_{\boldsymbol{\sigma}} \int \prod_{\mu} d\mu(z_\mu) \mathcal{B}_{N,K,\rho,\beta}^{(P)}(\boldsymbol{\sigma} | \boldsymbol{\xi}, \boldsymbol{\chi}; J, t).$$

A generalized average follows from this generalized measure as

$$\omega_t(\cdot) := \frac{1}{\mathcal{Z}_{N,K,\rho,\beta}^{(P)}(\boldsymbol{\xi}, \boldsymbol{\chi}; J, t)} \sum_{\boldsymbol{\sigma}} \cdot \mathcal{B}_{N,K,\rho,\beta}^{(P)}(\boldsymbol{\sigma} | \boldsymbol{\xi}, \boldsymbol{\chi}; J, t) \quad (3.9)$$

and

$$\langle \cdot \rangle_t := \mathbb{E}[\omega_t(\cdot)]. \quad (3.10)$$

Of course, when  $t = 1$  the standard Boltzmann measure and related averages are recovered.

As anticipated, the following analytical results are obtained under the *replica symmetry* assumption, namely assuming the self-averaging property for any order parameter  $X$ , i.e. the fluctuations around their expectation values vanish in the thermodynamic limit. In distributional sense, this corresponds to assuming

$$\lim_{N \rightarrow \infty} \mathcal{P}(X) = \delta(X - \bar{X}) \quad (3.11)$$

where  $\bar{X} = \langle X \rangle_t$  is the expectation value w.r.t. the interpolating measure. Hereafter, in order to lighten the notation, we drop the subscript  $t$  in the average symbol.

En route toward the self-consistency equations for the order parameters, we need to take the thermodynamic limit of the statistical pressure and, to this task, we must split the discussion into two cases: the ultra-storage regime  $b = P - 1$ , discussed in the following subsection- and ultra-tolerance regime  $b < P - 1$ , tackled in the subsequent one.

### 3.1 Ultra-storage capacity limit

In this subsection we study the network at work with the maximum storage of archetypes it can afford. In this ultra-storage regime of operation the signal-to-noise to be preserved is the standard one, i.e. the signal can not be lower than the noise.

**Proposition 1.** (*Ultra storage regime*) *In the thermodynamic limit ( $N \rightarrow \infty$ ) and under RS assumption, the quenched statistical pressure for the dense, supervised Hebbian network for even  $P \geq 4$  in high storage regime  $b = P - 1$  reads as*

$$\begin{aligned} \mathcal{A}_{\rho, r, \beta}^{(P)}(\alpha_{P-1}; J) = \mathbb{E} \left\{ \ln \left[ 2 \cosh \left( J + \beta' \frac{P}{2} \frac{(1+\rho)^{P/2-1}}{r} \bar{n}^{P-1} \hat{\chi}_M + Y \beta' \mathcal{V} \sqrt{\alpha_{P-1} \frac{P}{2} \bar{q}^{P-1}} \right) \right] \right\} + \\ + \frac{(\beta' \mathcal{V})^2 \alpha_{P-1}}{4} (1 - \bar{q}^P) + \frac{\beta'}{2} (1 + \rho)^{P/2} (1 - P) \bar{n}^P - (\beta' \mathcal{V})^2 \alpha_{P-1} \frac{P}{4} \bar{q}^{P-1} (1 - \bar{q}). \end{aligned} \quad (3.12)$$

with  $\mathbb{E} = \mathbb{E}_\chi \mathbb{E}_Y$  and  $\hat{\chi}_M = \frac{1}{M} \sum_{a=1}^M \chi_i^{1,a}$  and  $\bar{n}$  and  $\bar{q}$  fulfills the following self-consistent equations

$$\begin{aligned} \bar{n} = \frac{1}{r(1+\rho)} \mathbb{E} \left\{ \tanh \left[ \beta' \frac{P}{2} \frac{(1+\rho)^{P/2-1}}{r} \bar{n}^{P-1} \hat{\chi}_M + Y \beta' \mathcal{V} \sqrt{\alpha_{P-1} \frac{P}{2} \bar{q}^{P-1}} \right] \hat{\chi}_M \right\}, \\ \bar{q} = \mathbb{E} \left\{ \tanh^2 \left[ \beta' \frac{P}{2} \frac{(1+\rho)^{P/2-1}}{r} \bar{n}^{P-1} \hat{\chi}_M + Y \beta' \mathcal{V} \sqrt{\alpha_{P-1} \frac{P}{2} \bar{q}^{P-1}} \right] \right\}. \end{aligned} \quad (3.13)$$

Furthermore, considering the auxiliary field  $J$  linked to  $\bar{m}$  as  $\bar{m} = \nabla_J \mathcal{A}_{\rho, \beta, r, \alpha_{P-1}}^{(P)}(J) \Big|_{J=0}$ , we have

$$\bar{m} = \mathbb{E} \tanh \left[ \beta' \frac{P}{2} \frac{(1+\rho)^{P/2-1}}{r} \bar{n}^{P-1} \hat{\chi}_M + Y \beta' \mathcal{V} \sqrt{\alpha_{P-1} \frac{P}{2} \bar{q}^{P-1}} \right]. \quad (3.14)$$

For the proof we refer to Appendix B.

### 3.2 Ultra-noise tolerance limit

In this subsection, instead, we sacrifice memory storage to inspect a peculiarity of dense networks [3]: these networks, away from the saturation regime, can work at signal-to-noise that are prohibitive for standard pairwise Hopfield models.

**Proposition 2.** (*Ultra-noise tolerance regime*) *In the thermodynamic limit ( $N \rightarrow \infty$ ) under RS assumption, the quenched statistical pressure for the dense, supervised Hebbian network for even  $P \geq 4$  and a low storage load  $b < P - 1$  reads as*

$$\mathcal{A}_{\rho, r, \beta, \alpha_b}^{(P)}(J) = \mathbb{E} \left\{ \ln \left\{ 2 \cosh \left[ J + \beta' \frac{P}{2} \frac{(1+\rho)^{P/2-1}}{r} \bar{n}^{P-1} \hat{\chi}_M \right] \right\} + \frac{\beta'}{2} (1 + \rho)^{P/2} (1 - P) \bar{n}^P \right\} \quad (3.15)$$

with  $\mathbb{E} = \mathbb{E}_\chi$  and  $\bar{n}$  fulfills the following self-consistent equation

$$\bar{n} = \frac{1}{r(1+\rho)} \mathbb{E} \left\{ \tanh \left[ \beta' \frac{P}{2} \frac{(1+\rho)^{P/2-1}}{r} \bar{n}^{P-1} \hat{\chi}_M \right] \hat{\chi}_M \right\}. \quad (3.16)$$

Furthermore, considering the auxiliary field  $J$  linked to  $\bar{m}$  as  $\bar{m}$  as  $\bar{m}$  as  $\bar{m} = \nabla_J \mathcal{A}_{\rho, \beta, r, \alpha_b}^{(P)}(J) \mid_{J=0}$ , we have

$$\bar{m} = \mathbb{E} \left\{ \tanh \left[ \beta' \frac{P}{2} \frac{(1+\rho)^{P/2-1}}{r} \bar{n}^{P-1} \hat{\chi}_M \right] \right\}. \quad (3.17)$$

The proof is similar to the one presented in Appendix B for the high load regime, therefore we omit it.

**Remark 3.** *Ultra-noise tolerance: as already done in [1] for the unsupervised case, also in the supervised regime one can ask if this model is robust versus other kinds of noise affecting directly the synaptic processes.*

*It is possible to show that if we lower the maximum load (i.e. we let the network work at  $b < P-1$ ), the synaptic tensor could be affected by a supplementary extensive noise,  $w = \tau N^\delta$ , with  $\tau \in \mathbb{R}$  and  $\delta \in \mathbb{R}^+$ , such that*

$$\sum_{a_1, \dots, a_P} \eta_{i_1}^{\mu, a_1} \cdots \eta_{i_P}^{\mu, a_P} \rightarrow \sum_{a_1, \dots, a_P} \eta_{i_1}^{\mu, a_1} \cdots \eta_{i_P}^{\mu, a_P} + w \tilde{\eta}_{i_1, \dots, i_P}^{\mu, a_1, \dots, a_P} \quad \text{with} \quad \tilde{\eta}_{i_1, \dots, i_P}^{\mu, a_1, \dots, a_P} \sim \mathcal{N}(0, 1).$$

*If  $\delta = \frac{P-1-b}{2}$ , we recover exactly the expressions of high storage regime, namely Eqs. (3.13), as long as we replace  $\beta'$  with  $\beta' \tau$ . Whereas, for lower values of  $\delta$ , we remain in the low-load scenario depicted by Eq. (3.16). For an exhaustive description of the computation we please refer to [1], where we have lingered on the details for the unsupervised regime. The treatment of the supervised regime is analogous.*

### 3.3 Low entropy datasets

As explained in Sec. 3, the parameter  $\rho = (1-r^2)/(Mr^2)$  quantifies the amount of information needed to describe the original message  $\xi^\mu$  given the set of related examples  $\{\eta_a^\mu\}_{a=1, \dots, M}$ . In this section we focus on the case  $\rho \ll 1$  that corresponds to a low-entropy dataset or, otherwise stated, to a high-informative dataset.

The advantage of this analysis is two-fold: first, under this condition we obtain a relation between  $\bar{n}$  (a natural order parameter of the model) and  $\bar{m}$  (a practical order parameter of the model<sup>6</sup>), thus, the self-consistent equation for  $\bar{n}$  can be recast into a self-consistent equation for  $\bar{m}$  and its numerical solution versus the control parameters allows us to get the phase diagram for the system more straightforwardly. Second, the self-consistent equation for  $\bar{m}$  can be directly compared with an expression obtained from the stability analysis approach (developed for  $\rho \ll 1$  and  $T \rightarrow 0$ ) in such a way that we can finally estimate  $\mathcal{V}$ , see Sec. 4.1.

As explained in Appendix B, we start from the self-consistent equations found in the ultra-storage regime (3.13)-(3.14) and we exploit the CLT to write  $\hat{\chi}_M/r \sim 1 + \lambda \sqrt{\rho}$ . In this way we reach the simpler expressions

$$(1+\rho)\bar{n} = \bar{m} + \beta' \frac{P}{2} \rho (1+\rho)^{P/2-1} (1-\bar{q}) \bar{n}^{P-1}, \quad (3.18)$$

$$\bar{q} = \mathbb{E}_z [\tanh^2 g(\beta, Z, \bar{n})], \quad (3.19)$$

$$\bar{m} = \mathbb{E}_z [\tanh g(\beta, Z, \bar{n})], \quad (3.20)$$

---

<sup>6</sup>It is worth recalling that the model is supplied only with examples – upon which  $\{n^{\mu, a}\}$  are defined – while it is not aware of archetypes – upon which  $\{m^\mu\}$  are defined. The former constitute natural order parameters and, in fact, the Hamiltonian  $\mathcal{H}_{N, K, M}^{(P)}$  in (2.4) can be written in terms of the example overlaps. The latter are practical order parameters through which we can assess the capabilities of the network.

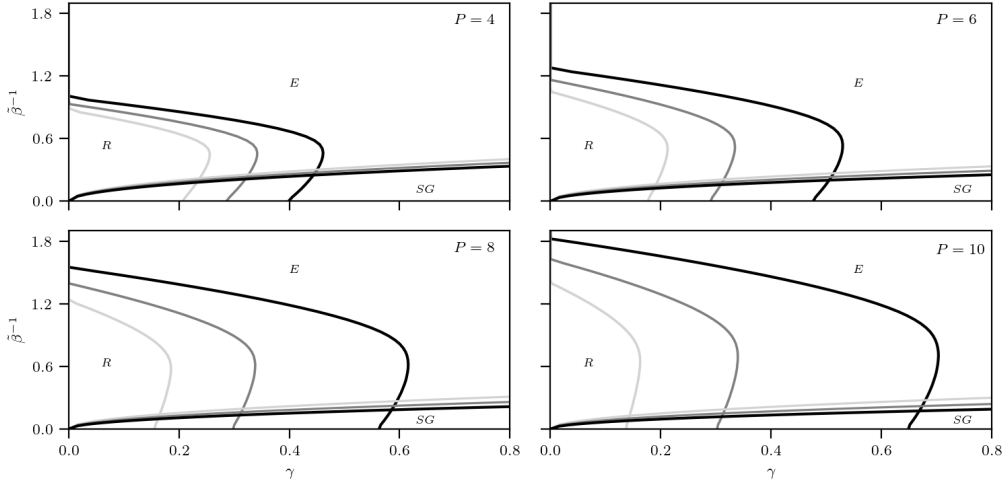


**Figure 2:** Phase diagrams of the dense Hebbian neural network, trained under supervised learning, at different values of  $P$  and its comparison to standard dense storing by  $P$ -spin Hopfield network (black dot line). In particular, in each panel we fix  $r = 0.2$  and two values of  $\rho$  (which are  $\rho = 0.1$  light gray and  $\rho = 0.05$  gray). We notice that, as  $P$  increases, retrieval zone of the phase diagrams are spreading. Moreover, the instability region, caused by the overlapping between retrieval and spin-glass regions, shrinks as  $P$  increases. Finally we note that the re-entrance of the computational phase transition delimiting the retrieval region is expected to be a pathology of the replica-symmetric solution, that should be removed by a RSB-scheme [10].

where

$$g(\beta, Z, \bar{n}) = \beta' \frac{P}{2} \bar{n}^{P-1} (1 + \rho)^{P/2-1} + \beta' Z \sqrt{\rho \frac{P^2}{4} \bar{n}^{2P-2} (1 + \rho)^{P-2} + \alpha_{P-1} \mathcal{V}^2 \frac{P}{2} \bar{q}^{P-1}} \quad (3.21)$$

and  $Z \sim \mathcal{N}(0, 1)$  is a standard Gaussian variable.

As a technical remark, we note that -as long as  $\rho \ll 1$ - we can truncate the right-hand-side of (3.18) into  $\bar{n}(1 + \rho) \sim \bar{m}$ . This results in a significant speed-up of numerical computations of self-consistency equations. In fact, by using  $\bar{n}(1 + \rho) = \bar{m}$ , in the argument of hyperbolic tangent, we get

$$g(\beta, Z, \bar{m}) = \tilde{\beta} \frac{P}{2} \bar{m}^{P-1} + Z \tilde{\beta} \sqrt{\rho \left( \frac{P}{2} \bar{m}^{P-1} \right)^2 + \alpha_{P-1} \frac{P}{2} \mathcal{V}^2 (1 + \rho)^P \bar{q}^{P-1}} \quad (3.22)$$

where we posed

$$\tilde{\beta} = \beta' (1 + \rho)^{-\frac{P}{2}} = \frac{2\beta}{P!} (1 + \rho)^{-\frac{P}{2}}. \quad (3.23)$$

The consequent, remarkable reward of this truncation consists in retaining only two of the three self-consistency equations, namely only the ones for  $\bar{q}$  and  $\bar{m}$ , while keeping the error (resulting in this truncation) numerically small for  $\tilde{\beta}^{-1}$  small (i.e. in the region of interest, where the network shows emergent computational capabilities, i.e. the retrieval region depicted in Figure 2). The validity of this approximation is further corroborated in Fig. 3 where we plot  $\bar{n}$  versus  $r$  for different values of  $\rho$ ,  $\alpha_{P-1} \mathcal{V}^2$  and  $\tilde{\beta}^{-1}$  and compare the outcomes obtained with and without the truncation.

With this truncation we also handle the Eqs. (3.18) and we compute their zero-temperature limit. Beyond an interest in the ground-state *per se*, here this analysis is pivotal because, combined with the results obtained by the stability analysis discussed in the next Sec. 4.1, it allows us to estimate the factor  $\mathcal{V}$  that appears in the self-consistency equations and whose knowledge is mandatory to solve those equations numerically. As detailed in the Appendix B, by taking the limit  $\beta \rightarrow \infty$  (i.e.,  $T \rightarrow 0$ ) in eqs. (3.18)-(3.20) we get

$$\bar{m} = \operatorname{erf} \left[ \frac{P}{2} \frac{\bar{m}^{P-1}}{G} \right],$$

$$G = \sqrt{2 \left[ \rho \left( \frac{P}{2} \bar{m}^{P-1} \right)^2 + \alpha_{P-1} \mathcal{V}^2 \frac{P}{2} (1 + \rho)^P \right]}, \quad (3.24)$$

$$\bar{q} = 1.$$

Finally, in Fig. 2 we plot phase diagrams obtained by solving these self-consistent equations for the Mattis magnetization and overlap for different values of  $\rho$  in supervised regime using (3.24): the three regions captured by the letters (R, SG, E) are respectively the *retrieval region* (where both the Mattis magnetization and the overlap are close to one), the *spin glass region* (where solely the overlap is close to one, but there is no longer Mattis magnetization) and the *ergodic region* (where both the order parameters are null). Further, it is also instructive to compare the computational phase transitions that split the phase diagram of these dense networks trained with supervised learning with the limiting phase transitions provided by standard Hebbian storing in dense networks: clearly the retrieval region of the latter works as an upper bound for the available retrieval regions by learning with noisy data. In the next section (see Fig. 4) indeed we prove that, in the large datasize limit, supervised Hebbian learning reaches the theoretical bound predicted by Hebbian storing (i.e. the amplitude of the various regions of their phase diagrams do coincide).

## 4 Numerical findings

### 4.1 Stability analysis and Monte Carlo simulations

In this section we adopt a different point of view in order to determine  $\mathcal{V}$  which is yet unknown. In particular by a stability analysis carried in the  $\beta \rightarrow \infty$  limit, we want to achieve again -but independently from the statistical mechanical route- the self consistency equations for the order parameters in order to compare them to those stemmed via the previous technique in the noiseless limit (i.e. Eqs. (3.24)). We suppose that the network is in a retrieval configuration, say  $\boldsymbol{\sigma} = \boldsymbol{\xi}^1$  without loss of generality, we evaluate the local field  $h_i(\boldsymbol{\xi}^1)$  acting on the generic neuron  $\sigma_i$ , and inspect if and when  $h_i(\boldsymbol{\xi}^1)\sigma_i > 0$  is satisfied for any  $i = 1, \dots, N$ : this is known as *stability analysis*.

Mirroring what we have done with the unsupervised dense Hebbian network presented in [1]. We start from the Hamiltonian (2.4), writing

$$-\beta' \mathcal{H}_{N,K,M,r}(\boldsymbol{\sigma}|\boldsymbol{\eta}) = \sum_{i=1}^N h_i(\boldsymbol{\sigma})\sigma_i, \quad (4.1)$$

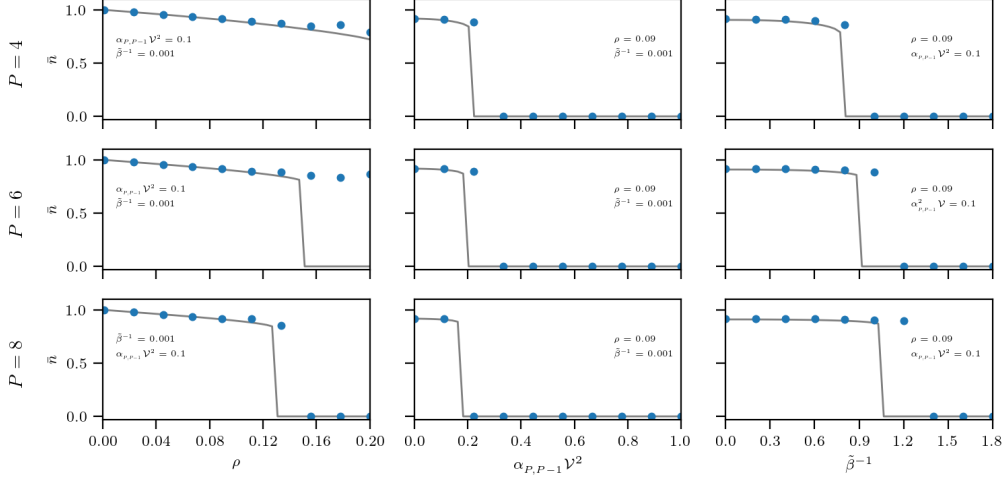


**Figure 3:** To check the goodness of the truncation we compute  $\bar{n}$  solving numerically (3.18)-(3.20) for different values of  $P$ ,  $\beta$ ,  $\alpha_{P-1}V^2$  and  $\rho$ . We compare the results obtained using the exact expression of  $\bar{n}$  (blue dots) and those obtained using the approximated one (namely  $\bar{n} = \bar{m}(1 + \rho)^{-1}$ , solid grey line). Although it does not seem entirely accurate, it is reasonable for our purposes, e.g. in  $T \rightarrow 0$  limit.

where the local fields  $h_i$  appear explicitly and are given by

$$h_i(\sigma) = \frac{\beta'}{2N^{P-1}M^P\mathcal{R}^{P/2}} \sum_{\mu=1}^K \sum_{i_2, \dots, i_P \neq i}^{N, \dots, N} \sum_{a_1, \dots, a_P}^{M, \dots, M} \xi_{i_1}^\mu \chi_{i_1}^{\mu, a_1} \dots \xi_{i_P}^\mu \chi_{i_P}^{\mu, a_P} \sigma_{i_2} \dots \sigma_{i_P}. \quad (4.2)$$

Reformulating the model in this fashion, the Monte Carlo updating rule for the spin configuration can be written as

$$\sigma_i^{(n+1)} = \sigma_i^{(n)} \text{sign} \left( \tanh \left[ \sigma_i^{(n)} h_i^{(n)}(\sigma^{(n)}) \right] + \Gamma_i \right) \quad \text{with } \Gamma_i \sim \mathcal{U}[-1; +1]. \quad (4.3)$$

Performing the zero fast-noise limit  $\beta' \rightarrow +\infty$ , we have

$$\sigma_i^{(n+1)} = \sigma_i^{(n)} \text{sign} \left( \sigma_i^{(n)} h_i^{(n)}(\sigma^{(n)}) \right). \quad (4.4)$$

Now we want to check the stability of the signal provided by the archetype  $\xi^1$ , so we start from the configuration  $\sigma^{(1)} = \xi^1$ . Then, the one-step MC approximation  $\sigma^{(2)}$  returns an expression for the Mattis magnetization that reads as

$$m_1^{(2)} = \frac{1}{N} \sum_{i=1}^N \xi_i^1 \sigma_i^{(2)} = \frac{1}{N} \sum_{i=1}^N \text{sign} \left( \xi_i^1 h_i^{(1)}(\xi^1) \right); \quad (4.5)$$

using the CLT on the variables  $\xi_i^1 h_i^{(1)}(\xi^1)$ , for  $i = 1, \dots, N$ , we get

$$\xi_i^1 h_i^{(1)}(\xi^1) \sim \mu_1 + z_i \sqrt{\mu_2} \quad \text{with } z_i \sim \mathcal{N}(0, 1) \quad (4.6)$$

where

$$\mu_1 := \mathbb{E}_\xi \mathbb{E}_\chi \left[ \xi_i^1 h_i^{(1)}(\boldsymbol{\xi}^1) \right], \quad (4.7)$$

$$\mu_2 := \mathbb{E}_\xi \mathbb{E}_\chi \left[ \{h_i^{(1)}(\boldsymbol{\xi}^1)\}^2 \right]. \quad (4.8)$$

Thus Eq. (4.5) becomes

$$m_1^{(2)} = \frac{1}{N} \sum_{i=1}^N \text{sign}(\mu_1 + z_i \sqrt{\mu_2}). \quad (4.9)$$

For large values of  $N$ , the arithmetic mean coincides with the expected value; thus we have

$$\frac{1}{N} \sum_{i=1}^N g(z_i) \text{ with } z_i \sim \mathcal{N}(0, 1) \xrightarrow[N \rightarrow \infty]{} \mathbb{E}[g(z)] = \int \frac{dz}{\sqrt{2\pi}} e^{-\frac{z^2}{2}} g(z). \quad (4.10)$$

Therefore, we can rewrite Eq. (4.5) as

$$m_1^{(2)} = \int \frac{dz}{\sqrt{2\pi}} e^{-\frac{z^2}{2}} \text{sign}(\mu_1 + z \sqrt{\mu_2}) = \text{erf} \left( \frac{\mu_1}{\sqrt{2(\mu_2 - \mu_1^2)}} \right). \quad (4.11)$$

We carry out the computations of  $\mu_1$  and  $\mu_2$  in Appendix C: hereafter we report only their values, which are

$$\mu_1 = \frac{\beta'}{2(1+\rho)^{P/2}}, \quad (4.12)$$

$$\mu_2 = \left( \frac{\beta'}{2(1+\rho)^{P/2}} \right)^2 [\alpha_{P-1}(2P-3)!!(1+\rho)^P + 1 + \rho]. \quad (4.13)$$

By replacing  $\mu_1$  and  $\mu_2$  in Eq. (4.11) with the r.h.s. of eq.s (4.12) (4.13), we get

$$m_1^{(2)} \sim \text{erf} \left( \frac{1}{\sqrt{2[\alpha_{P-1}(2P-3)!!(1+\rho)^P + \rho]}} \right). \quad (4.14)$$

In order to simplify the notation it is convenient to introduce the  $P$ -independent load  $\gamma$  defined by

$$\alpha_{P-1} := \gamma \frac{2}{P(2P-3)!!}. \quad (4.15)$$

We observe that, as long as  $P$  is fixed, the assumption  $\alpha_{P-1} < \infty$  also means that  $\gamma < \infty$ . Thus the expression of  $m_1^{(2)}$  becomes

$$m_1^{(2)} \sim \text{erf} \left( \frac{1}{\sqrt{2 \left[ \gamma \frac{2}{P} (1+\rho)^P + \rho \right]}} \right). \quad (4.16)$$

We can finally evaluate the parameter  $\mathcal{V}$ : via stability analysis we obtained

$$m_1^{(2)} \sim \text{erf} \left( \frac{1}{\sqrt{2 \left[ \gamma \frac{2}{P} (1+\rho)^P + \rho \right]}} \right), \quad (4.17)$$

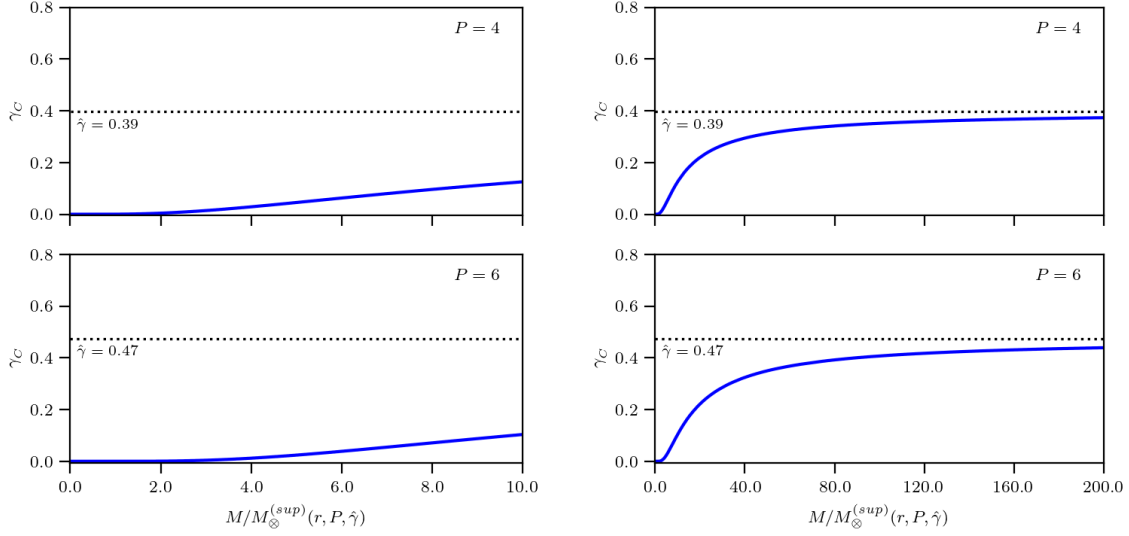


**Figure 4:** To inspect how the critical storage evolves as the dataset size varies, we numerically solve the self equations in the  $T \rightarrow 0$  limit, namely Eqs. (3.24), for  $r = 0.2$ . In the left column we plot the critical load  $\gamma_c$  (blue line) w.r.t. the ratio of the number of examples  $M$  and the lower bound of  $M$  for supervised regime (see Eq. (4.25)) for different degrees of interaction  $P = 4, 6$ : as  $\gamma_c$  detaches from zero a non-null retrieval region appears in the phase diagram. In the right column we inspect the large dataset size limit, namely we broaden the  $x$ -axis to inspect how  $\gamma_c$  increases with  $M$ : in particular, for  $M \gg M_{\otimes}^{(sup)}(r, P, \gamma = \hat{\gamma})$ , it saturates to the critical load  $(\hat{\gamma})$  predicted by the storage in the standard P-spin Hopfield network with the same interaction order [5] (represented by the horizontal dashed line).

while, from the self consistency equations in (3.24) for  $\beta \rightarrow \infty$  (i.e., we set  $\bar{m} \sim 1$  and  $\bar{q} \sim 1$ ), we had

$$\bar{m} \sim \text{erf} \left( \frac{1}{\sqrt{2} \left[ \gamma \frac{4}{P^2 (2P-3)!!} \mathcal{V}^2 (1+\rho)^P + \rho \right]} \right) \quad (4.18)$$

thus, to have a perfect match between the two equations, we have to fix the variance of the noise term, namely  $\mathcal{V}$ , as

$$\mathcal{V} = \sqrt{\frac{P(2P-3)!!}{2}}. \quad (4.19)$$

Therefore, Eq. (3.22) finally becomes

$$g(\gamma, \tilde{\beta}, Z) = \tilde{\beta} \frac{P}{2} \bar{m}^{P-1} + \tilde{\beta} Z \sqrt{\rho \left( \frac{P}{2} \bar{m}^{P-1} \right)^2 + \gamma \frac{P}{2} (1+\rho)^P \bar{q}^{P-1}}. \quad (4.20)$$

In order to corroborate the (stability analysis driven) estimate of  $\mathcal{V}$ , we have done numerical computations using MC simulations with Plefka's dynamics [25, 49]: discussion and results about this method are reported in Appendix D.

If the network has to retrieve one of the archetypes successfully, we need to require that this one-step MC magnetization is larger than  $\text{erf}(\Theta)$  where  $\Theta \in \mathbb{R}^+$  is a tolerance level, thus we obtain the criterion

$$\frac{1}{\left(\rho + \gamma \frac{2}{P} (1 + \rho)^P\right)} > \Theta. \quad (4.21)$$

that can be written as

$$1 > \Theta^2 \left(\rho + \gamma \frac{2}{P} (1 + \rho)^P\right). \quad (4.22)$$

Setting the confidence level  $\Theta = 1/\sqrt{2}$ , which corresponds to the fairly standard condition

$$\mathbb{E}_{\xi, \chi}[\xi_i^1 h_i^{(1)}(\xi^1)] > \sqrt{\text{Var}[\xi_i^1 h_i^{(1)}(\xi^1)]}$$

(see Eqs. (4.7), (4.8), (4.11)), the previous relation determines a lower bound for  $M$ , denoted as  $M_{\otimes}^{(\text{sup})}(r, P, \gamma)$ , that guarantees the signal to be prevailing over the noise.

We now discuss a few special cases under the assumption  $r \ll 1$  to inspect if the developed theory smoothly recovers known limits.

In the low-load regime  $\gamma = 0$ , the expression in (4.22) becomes

$$M > \frac{1}{2} \frac{(1 - r^2)}{r^2} \sim \frac{1}{2} \frac{1}{r^2} \implies M_{\otimes}^{(\text{sup})}(r, P, 0) = \frac{1}{2r^2} \quad (4.23)$$

where the last equality holds for  $r \ll 1$ : note that, as expected [44, 53], the power-law scaling  $M(r) \propto r^{-2}$  in the dataset threshold for learning is recovered.

If  $\gamma \neq 0$  and  $P = 2$ , the classic Hopfield picture is also recovered, as shown in [8]

$$M > \frac{\sqrt{\gamma}}{r^2 \sqrt{2}} \implies M_{\otimes}^{(\text{sup})}(r, 2, \gamma) = \sqrt{\frac{\gamma}{2}} \frac{1}{r^2}. \quad (4.24)$$

Finally, if  $\gamma \neq 0$  and  $P > 2$ , we have

$$M > \frac{\sqrt{\gamma}}{r^2 \sqrt{P}} \implies M_{\otimes}^{(\text{sup})}(r, P, \gamma) = \left(\frac{\gamma}{P}\right)^{1/P} \frac{1}{r^2}. \quad (4.25)$$

These results are corroborated by numerical simulations: in Fig. 4 we plot the number of examples  $M$  w.r.t.  $\gamma_C$  at different values of  $P$ . We recall that the critical load  $\gamma_C$  is the load beyond which a black-out scenario emerges, as predicted by Hebbian storing, namely  $\lim_{\gamma \rightarrow \gamma_C^-} \bar{m} \neq 0$  and  $\lim_{\gamma \rightarrow \gamma_C^+} \bar{m} = 0$ .

When  $M$  is chosen following the prescription in Eq. (4.25), supervised learning by Hebbian dense networks reaches the performances of standard storing by the P-spin Hopfield model, of the same density  $P$  (i.e. the two schemes give rise to the same retrieval region).

## 4.2 Application to structured dataset

In the previous sections we worked out the theory under the assumption of a random dataset scenario and we have shown general agreement with numerical simulations on unstructured datasets.

Now, we extend the numerics to cope with structured datasets: examples are no longer random, but the pixels in the images are correlated in order to create a real pattern [42]: in particular we explore MNist and Fashion MNist datasets.

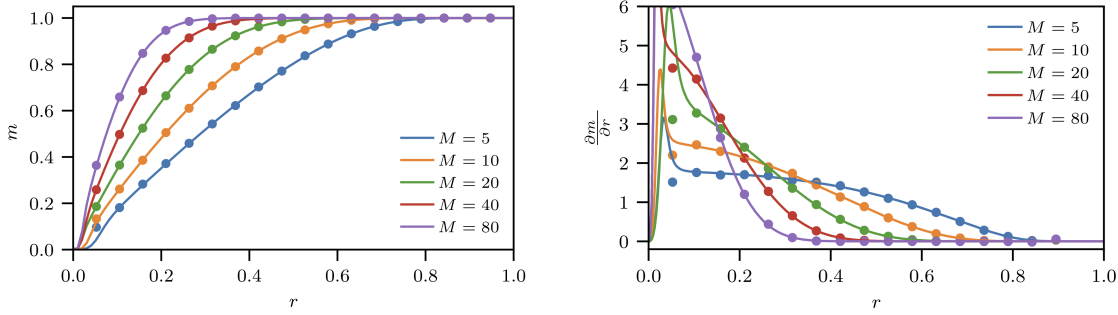


**Figure 5:** Comparisons between MC simulations equipped with Plefka dynamic (lines) and signal-to-noise analysis (dots). The number of examples  $M$  varies as specified by the legend, while the number of neurons and patterns are kept fixed at  $N = 500$ ,  $K = 400$ . As a consequence, the load is fixed below its critical value,  $\gamma < \gamma_c$ . The simulations concern the supervised regime with degree of interaction  $P = 4$  and confirm the goodness of the signal-to-noise estimation of  $\mathcal{V}$ , namely equation (4.19). In particular, we report the archetype magnetization  $m$  and its susceptibility  $\partial_r m$  at various training set sizes  $M$  by making the noise  $r$  in the training set vary from 0, where all the example are pure random noise, to 1, where there is no difference among examples and archetype. We note that in the small noise limit  $r \rightarrow 0$  the network always perfectly retrieves the archetype as expected, whereas, for  $r \rightarrow 1$ , no retrieval is possible. We notice that, when  $m > 0.1$ , the signal to noise analysis perfectly captures the behaviour of the susceptibility predicted by Plefka dynamics.

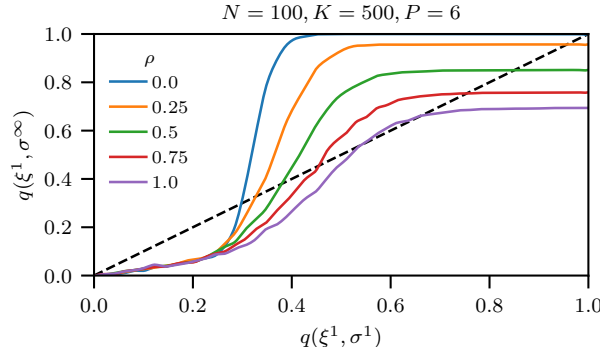


**Figure 6:** Investigation of the basins of the attractors for ideal patterns with MC simulations mixed with Plefka's dynamics by a dense network built of by  $N = 100$  neurons, interacting with a density  $P = 6$  and handling  $K = 500$  patterns. On the horizontal axes we plot the overlap between the initial network's configuration and the first pattern (with no loss of generality) while on the vertical axes we plot the overlap between the final configuration reached by the neural dynamics and the same pattern. We stress that, monotonically, as the entropy in the dataset  $\rho$  increases (hence the dataset contains less and less information), the width of basins for the attractors shrinks.

We recall that MNist is a dataset for image classification built up of handwritten single digits, has a training set of 60,000 examples, and a testing set of 10,000 examples [29]. This dataset is made of

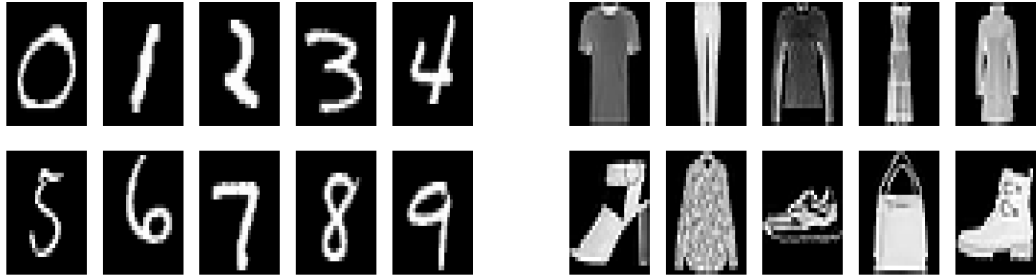


**Figure 7:** In this figure we report one example chosen at random from each class contained in MNist (Left) and Fashion MNist (Right) datasets.

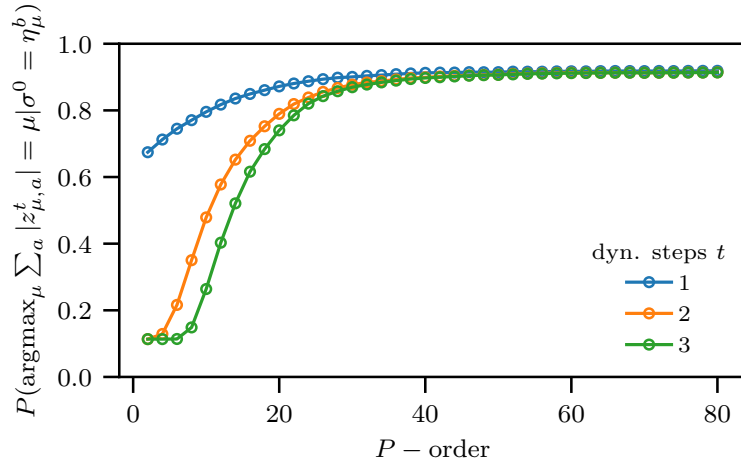


**Figure 8:** In this figure we face up to MNIST dataset classification using the scheme expressed in Sec. 4.2. We notice that performances using a single step of MC dynamic are better and it displays a plateau when the grade of interaction  $P$  increases. This imply that very higher order dense networks do not benefit from the tools.

square  $28 \times 28$  pixel grayscale images, with the center of mass of the pixels at the center of the  $28 \times 28$  field.

Fashion-MNIST, analogously, comprises  $28 \times 28$  grayscale images of 70,000 fashion products from 10 categories, it shares with the MNIST dataset the same image size, data format and the structure of training and testing splits [56]. By way of example, in Fig. 7 an example from each class in MNist (left) and Fashion MNist dataset (right) are shown.

In order to understand the procedure of classification further notions are in order: from now on we will indicate the structured dataset as  $\{\zeta^{\mu,a}\}_{a=1,\dots,M}^{\mu=1,\dots,K}$ , with  $\zeta^{\mu,a} \in \mathbb{R}^N$ , where  $\mu$  labels the different classes and  $a$  labels the items pertaining to the same class.

Before designing the network and inspecting its performances, data must be binarized, namely we associate a new dataset where each entry is binary  $\{\eta^{\mu,a}\}_{a=1,\dots,M}^{\mu=1,\dots,K}$ ,  $\eta^{\mu,a} \in \{-1, 1\}^N$ . For each pixel  $i$

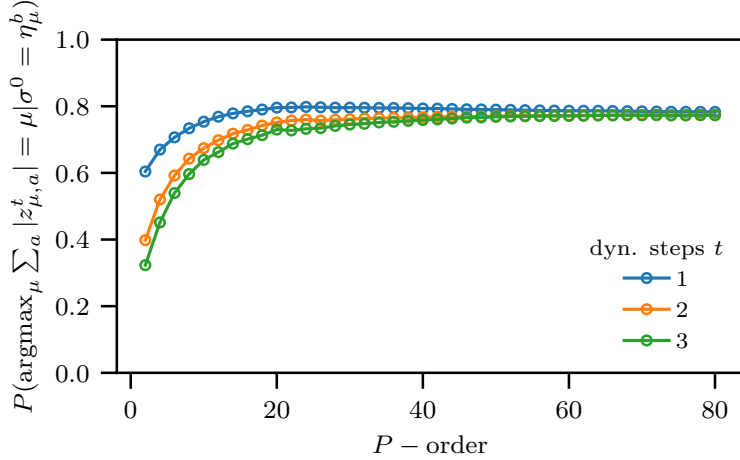


**Figure 9:** We repeat the classification as done in Fig. 8 for MNist dataset also for Fashion MNist one. In this case we find the maximum for small values of the grade of interaction  $P$  and performance for a single step of MC dynamics are better. For bigger values of  $P$  also in this case we have a plateau.

we evaluate the average  $\bar{\zeta}_i$  over  $\mu$  and over  $a$ , that is

$$\bar{\zeta}_i = \frac{1}{KM} \sum_{\mu=1}^K \sum_{a=1}^M \bar{\zeta}_i^{\mu,a} \quad (4.26)$$

and set

$$\eta_i^{\mu,a} = \begin{cases} +1 & \text{if } \bar{\zeta}_i^{\mu,a} > \bar{\zeta}_i, \\ -1 & \text{if } \bar{\zeta}_i^{\mu,a} < \bar{\zeta}_i. \end{cases} \quad (4.27)$$

The original dataset  $\{\zeta_i^{\mu,a}\}_{a=1, \dots, M}^{\mu=1, \dots, K}$  has therefore been mapped into a new binary dataset  $\{\eta_i^{\mu,a}\}_{a=1, \dots, M}^{\mu=1, \dots, K}$ .

Now, for each class, we assess the related quality denoted as  $r_\mu$  and obtained as follows: given  $i$  and  $\mu$ , we count the number of positive  $N_{i,\mu}^+$  and negative  $N_{i,\mu}^-$  pixels over the class sample  $\eta_i^{\mu,a}$

$$r_\mu = \frac{1}{N} \sum_{i=1}^N \frac{|N_{i,\mu}^+ - N_{i,\mu}^-|}{N_{i,\mu}^+ + N_{i,\mu}^-}, \quad (4.28)$$

then exploiting the relation  $\rho = \frac{1-r^2}{r^2 M}$ , for an arbitrary  $\rho \in \mathbb{R}^+$ , we introduce

$$M_\mu = \frac{1-r_\mu^2}{r_\mu^2 \rho} \quad (4.29)$$

that represents the number of items needed to correctly process the  $\mu$ -th class.

In order to show how this procedure works, an example from real and binary MNist dataset are shown in Fig. 10.

To check the network performances in classifying these structured datasets we rely upon the integral expression of the partition function (see eq. 3.1), namely we use the dual representation of the

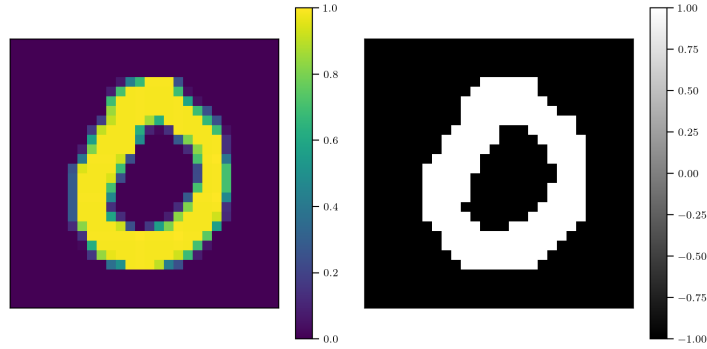


**Figure 10:** In this figure we report an example from the original real MNist dataset  $\{\zeta^{\mu,a}\}_{a=1,\dots,M}^{\mu=1,\dots,K}$ , a zero in particular, (left) and its binary version (right), from the new dataset  $\{\eta^{\mu,a}\}_{a=1,\dots,M}^{\mu=1,\dots,K}$ .

network in terms of a generalized restricted Boltzmann machine, as discussed in Remark 1: in this representation the network has an input visible layer of size  $N = 784$ , corresponding to the number of pixels of each item and whose neurons are denoted as  $\sigma = (\sigma_1, \dots, \sigma_N)$ , and it also has a hidden layer of size  $K = 10$ , corresponding to the overall number of classes and whose neurons are denoted as  $z = (z_1, \dots, z_K)$ : note that we train the machine in the grandmother-cell setting, namely by assigning to each hidden neuron a specific archetype to recognize -one per neuron-, as this guarantees that -by marginalizing the partition function over the hidden neurons- the dense Hebbian network has the archetypes as candidate minima of its memory landscape. Finally, just as a matter of practical convenience, coupled to this hidden layer, the network got an output visible layer of the same size  $K$  and whose neurons are denoted as  $\pi = (\pi_1, \dots, \pi_K)$  which is a softmax layer relating  $\pi_\mu$  with the probability that the input supplied to the network belongs to the  $\mu$ -th class.

Let us now specify the activation functions of the hidden and of the output neurons. Exploiting the Plefka dynamics equations (D.15) - (D.16) “in tandem” to make the system evolve, we start from an initial configuration  $\sigma^{(0)}$  initializing the visible layer as  $\sigma^{(0)} = \eta^{\mu,b}$ , where  $\eta^{\mu,b}$  pertains to the  $\mu$ -th class, then we evaluate the related  $z_\mu^{(0)}$  for any  $\mu$  and we use them in Eq. (D.15) to get  $m_i^{(0)}$  for any  $i$ , the latter is then used in Eq. (D.16) to get  $z_\mu^{(1)}$ , and we proceed this way, bouncing from (D.15) to (D.16), for a few iterative steps of such dynamics. Finally the goodness of the classification process is checked with the output layers which is determined as  $\pi_\mu = \text{softmax}(|z|)$  which returns the classification probability for the input; the absolute value of the hidden neuron is carried out element-wise and it is meant to preserve the gauge invariance characterizing the model. We recall that in the softmax layer is applied with a free parameter denoted with  $\theta$ , that is

$$\pi_\mu(|z^{(t)}|) = \frac{e^{\theta|z_\mu^{(t)}|}}{\sum_{\nu=1}^K e^{\theta|z_\nu^{(t)}|}}, \quad (4.30)$$

where the apex  $(t)$  refers to the number of steps made with Plefka dynamics, and  $\theta$  tunes the broadness of the distribution, playing a role similar to the temperature in the statistical mechanics framework. If we let  $\theta \rightarrow \infty$  the softmax collapses to a delta function peaked at  $\text{argmax}_{\mu=1,\dots,K}(|z|)$ . As  $\theta \rightarrow \infty$ , we identify the probability of correctly classifying a given example as

$$P_+ = \pi_\mu(\sigma^{(0)} = \eta^{\mu,b}) = P\left(\text{argmax}_\mu(|z^{(t)}|) = \mu | \sigma^{(0)} = \eta^{\mu,b}\right) \quad (4.31)$$

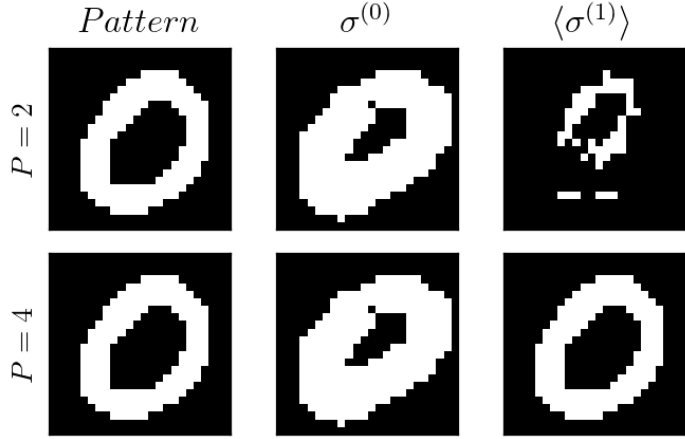


**Figure 11:** In this picture we show the power of dense supervised Hebbian networks in reconstruction of a pattern from a given example of MNist dataset. Indeed, the first column is the pattern, a zero, built as the arithmetic mean of  $M = 12$  examples. In the second one there is the initial configuration of the chosen example. Finally, in the third column there are the reconstructions with classic RBM and a single step MC dynamics equipped with Plefka’s dynamic with  $P = 2$  (top) and  $P = 4$  (down). We highlight that, even only with  $P = 4$ , performances are by far better.

(this probability is shown by varying the parameter  $P$  in Figs. 8 and 9 respectively for MNist and Fashion MNist dataset), and instead with

$$P_- = \pi_\mu(\boldsymbol{\sigma}^{(0)} = \boldsymbol{\eta}^{\nu \neq \mu, b}) = P\left(\operatorname{argmax}_\mu(|\mathbf{z}^{(t)}|) = \mu | \boldsymbol{\sigma}^{(0)} \neq \boldsymbol{\eta}^{\mu, b}\right) \quad (4.32)$$

the class-specific probability of misclassifying a given example. These probabilities are normalised as  $P_+ + 9P_- = 1$  since in total there are 10 different classes for both datasets.

Let us discuss results on network’s performance: we have done classification using the aforementioned scheme for both MNist and Fashion MNist datasets. Now we start from the first one.

As showed in Fig. 8, we notice that the retrieval is not perfect as the random case but it seems to improve as the order of interaction  $P$  of the network increases. Moreover using Hinton’s one single step of dynamics [54] seems convenient, especially for small values of  $P$ .

We have applied the same procedure done for MNist dataset to Fashion MNist one: see Figure 9. We can see that the results are a bit worse than those on MNist dataset in terms of retrieval. This could be related to the presence of an elevated number of details which increase the structure of the images; moreover, several details are lost during the binarization. However, also in this dataset we can state that using one single step of dynamic gives us better performances.

By way of example how the network works, we show in Fig. 11 a reconstruction of a pattern starting from an example of MNist dataset with different values of  $P$ . We notice how performances improve already using  $P = 4$ .

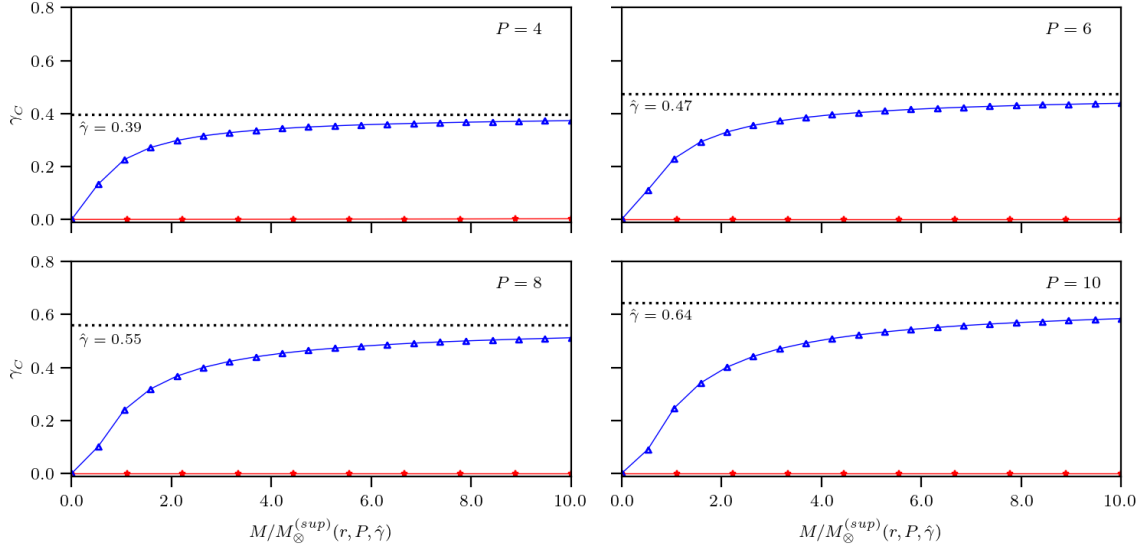


**Figure 12:** We show the comparison of performances in null-temperature limit between unsupervised (red stars) and supervised (blue triangles) with  $r = 0.2$  when the minimum number of examples to have a retrieval region scales as found in supervised regime from analytical computation in Sec. (3.3) (namely  $M > M_0(r, P, \gamma)$ ). We also represent in the figure dense associative network's performance (dot) as predicted by Hebbian storing.

### 4.3 Comparison between unsupervised and supervised regime

The purpose of this section is to compare dense Hebbian neural networks in unsupervised and supervised regime. For the exhaustive description of the unsupervised regime we remind to [1].

In a nutshell, both of this networks are made of  $N$  neurons whose interaction is in groups of  $P$  units regulated differently, reads as

$$J_{i_1 i_2 \dots i_P}^{unsup} \sim \frac{1}{MN^{P-1}} \sum_{\mu=1}^K \sum_{a=1}^M \eta_{i_1}^{\mu, a} \dots \eta_{i_P}^{\mu, a}, \quad (4.33)$$

$$J_{i_1 i_2 \dots i_P}^{sup} \sim \frac{1}{M^P N^{P-1}} \sum_{\mu=1}^K \sum_{a_1, \dots, a_P=1}^{M, \dots, M} \eta_{i_1}^{\mu, a_1} \dots \eta_{i_P}^{\mu, a_P} \quad (4.34)$$

where  $\{\eta_a^\mu\}_{a=1, \dots, M}^{\mu=1, \dots, K}$  represent perturbed versions of the unknown archetypes  $\{\xi^\mu\}_{\mu=1, \dots, K}$ . In the former expression there is no teacher that knows the labels and can thus cluster the examples archetype-wise as it happens in the latter, this is why the two generalizations are associated to, respectively, unsupervised and supervised protocols [5, 12].

Focusing on analytical results, reached through statistical mechanics techniques, we stress that either in unsupervised or in supervised regimes there is a distinction between high and low storage regime.

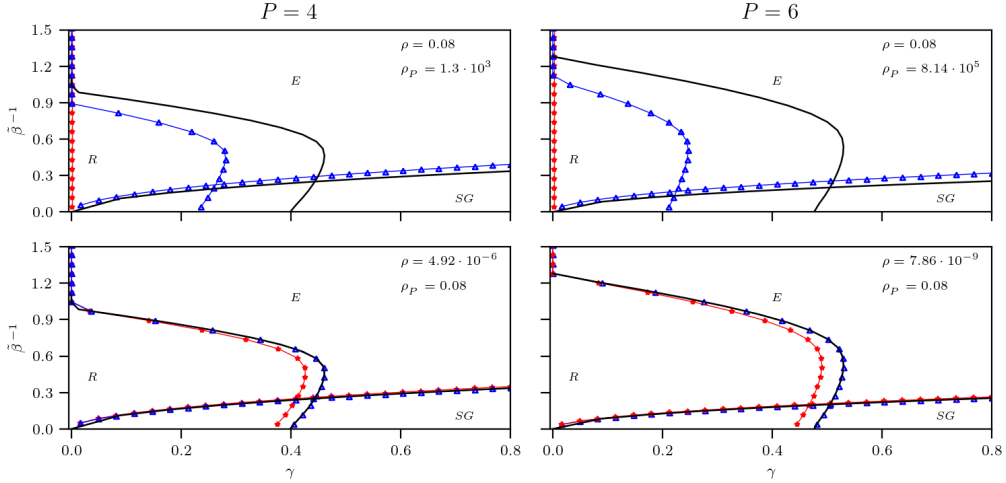


**Figure 13:** In this figure we show a comparison between supervised (blue triangles) and unsupervised (red stars) phase diagrams for  $r = 0.2$  considering  $P = 4$  (left) and  $P = 6$  (right). For each  $P$ , in the first and second row we choose the correct value of  $M$  (see Eq. (4.39)) to keep fixed to the value of 0.08 respectively  $\rho$  and  $\rho_P$ . Note that, as long as  $\rho_P \sim \mathcal{O}(1)$  also  $\rho \sim \mathcal{O}(1)$  thus, fixed the dataset quality, if the unsupervised model has a non-null retrieval region, also the supervised model has a non-null retrieval region (while clearly -as shown in the first row- the contrary is not the case). Moreover, we highlight that the retrieval region of the supervised regime is always bigger than the unsupervised one and both the models of learning -for  $M \rightarrow \infty$  (namely  $\rho, \rho_P \rightarrow 0$ )- approach the phase diagram of the standard Hebbian storage by the P-spin Hopfield model (solid black line).

Indeed, in the former we reach the following expressions for quenched statistical pressure

$$\mathcal{A}_{\beta, r, \gamma}^{(P, unsup)}(Y) = \mathbb{E} \left\{ \ln 2 \cosh \left[ \tilde{\beta} \frac{P}{2} \bar{n}^{P-1} (1+\rho)^{P-1} \frac{\hat{\chi}_M}{r} + Y \tilde{\beta} \sqrt{\gamma (1+\rho_P) \frac{P}{2} \bar{q}^{P-1}} \right] \right\} + \frac{\tilde{\beta}^2}{4} \gamma (1+\rho_P) (1-\bar{q}^P) - \frac{\tilde{\beta}}{2} (P-1) (1+\rho)^P \bar{n}^P - \frac{\tilde{\beta}^2}{4} \gamma P (1+\rho_P) \bar{q}^{P-1} (1-\bar{q}), \quad (4.35)$$

$$\mathcal{A}_{\beta, r, \gamma}^{(P, sup)}(Y) = \mathbb{E} \left\{ \ln \left[ 2 \cosh \left( \tilde{\beta} \frac{P}{2} (1+\rho)^{P-1} \bar{n}^{P-1} \frac{\hat{\chi}_M}{r} + Y \tilde{\beta} \sqrt{\gamma \frac{P}{2} (1+\rho)^P \bar{q}^{P-1}} \right) \right] \right\} + \frac{\tilde{\beta}^2 \gamma}{4} (1+\rho)^P (1-\bar{q}^P) - \frac{\tilde{\beta}}{2} (P-1) (1+\rho)^P \bar{n}^P - \frac{\tilde{\beta}^2}{4} \gamma P (1+\rho)^P \bar{q}^{P-1} (1-\bar{q}) \quad (4.36)$$

where  $\mathbb{E} = \mathbb{E}_Y \mathbb{E}_\chi$  and  $\tilde{\beta} = \beta' (1+\rho)^{-P/2}$ .

The most important feature to be underlined concerns the number of examples network needs w.r.t. the quality of the dataset  $r$  in order to have a non null retrieval region and to generalize the archetypes from their perturbed version.

If  $\gamma \neq 0$  we have

$$M_\otimes^{(sup)}(r, P, \gamma) \sim \left( \frac{\gamma}{P} \right)^{1/P} \frac{1}{r^2} = \left( \frac{\gamma}{P} \frac{1}{r^{2P}} \right)^{1/P}, \quad (4.37)$$

$$M_\otimes^{(unsup)}(r, P, \gamma) \sim \frac{\gamma}{P r^{2P}} = \left[ M_\otimes^{(sup)}(r, P, \gamma) \right]^P \quad (4.38)$$

where  $M_{\otimes}^{(sup)}(r, P, \gamma)$  represents a lower bound for the minimal amount of examples required by the network to accomplish learning (and thus storage and retrieval in future usage). This means that the number of examples required in unsupervised regime is extensively higher than supervised one. Moreover, since  $r \in (0, 1)$  and  $\gamma > 0$ , the number of examples in supervised regime is always less than that one in unsupervised regime where  $P \geq 2$  even: supervised learning allows to work even when small datasets are available, still achieving by far better performances if compared with the unsupervised counterpart.

After the analytical description, let us focus on numerical results.

In Fig. 12 we compare the phase diagrams of dense networks achieved in unsupervised vs supervised regimes. We stress that, with the lower bound  $M_{\otimes}^{(sup)}$  for supervised case as recovered in Eq. (4.25), the unsupervised model cannot manage to do retrieval. Indeed, as expected from our analytical analysis (see Eqs. (4.37)-(4.38)),  $M_{\otimes}^{(sup)}$  is much smaller than its unsupervised counterpart, namely  $M_{\otimes}^{(unsup)}$ <sup>7</sup>.

In order to preserve network's abilities, as long as we have  $r \ll 1$ , the dataset size for the supervised and unsupervised model have to scale respectively according to the relations

$$M^{(sup)} \sim r^{-2} \quad \text{and} \quad M^{(unsup)} \sim r^{-2P}. \quad (4.39)$$

This is equivalent to set  $\rho \sim \mathcal{O}(1)$  and  $\rho_P \sim \mathcal{O}(1)$ . If we fix the dataset quality  $r$ , and we use a number of examples that leads to a non-null retrieval region for the unsupervised model, then we also always have a non-null supervised retrieval region. However the contrary is not the case, as shown in Fig. 13, supporting the fact that the presence of supervision in learning dramatically improves learning outcomes.

## 5 Conclusion and outlooks

In this paper we investigated the dense Hopfield neural network endowed with supervised Hebbian couplings. The theory is analytically developed at work with random and structureless datasets, but it is numerically corroborated also with MNist [29] and Fashion MNist [56] stuctured datasets. We recall that the network is made of  $N$  neurons that interact in groups of  $P$  units with a strength encoded by the tensor  $\mathbf{J}^{sup}$ , whose generic entry (retaining only the highest order) reads as

$$\mathbf{J}_{i_1 i_2 \dots i_P}^{sup} \sim \frac{1}{M^P N^{P-1}} \sum_{\mu=1}^K \sum_{a_1, \dots, a_P=1}^{M, \dots, M} \eta_{i_1}^{\mu, a_1} \dots \eta_{i_P}^{\mu, a_P} \quad (5.1)$$

where  $\{\boldsymbol{\eta}^{\mu}\}_{a=1, \dots, M}^{\mu=1, \dots, K}$  is the dataset, made of  $K$  subsets of examples, labelled by  $a$ , referred to  $K$  unknown archetypes  $\{\boldsymbol{\xi}^{\mu}\}_{a=1, \dots, M}^{\mu=1, \dots, K}$ . The quality of the dataset is determined by  $r$ , and we recover the standard dense Hopfield model by setting  $M = 1$  and  $r = 1$ .

Hereafter we summarize the main outcomes of our work. Some of them are shared with the unsupervised counterpart, whose analysis appeared in the twin paper [1]:

1. The *ultra-storage regime* of the dense Hebbian neural network, characterized by a number of storable archetypes that grows as  $K \sim N^{P-1}$ , is preserved when the standard Hebbian coupling for storing is replaced by the Hebbian coupling for supervised learning. One can still introduce a load  $\alpha_{P-1} = \lim_{N \rightarrow \infty} \frac{K}{N^{P-1}}$  and determine its critical dataset-dependent value beyond which a black-out scenario emerges.

<sup>7</sup>In [1] it is also discussed what happens when we do not respect this lower bound for unsupervised regime.

2. There exists a (quality dependent  $r$ ) threshold value  $M_{\otimes}(r)$ , for the minimal dataset size  $M$  allowing archetype's learning (and thus its storage and successive retrieval), that has a power-law scaling as  $M_{\otimes}^{(sup)}(r, P, \gamma) \sim 1/r^2$ . The fact that this threshold value does not increase with  $P$  is a main difference w.r.t. learning in an unsupervised regime and highlights how learning by dense networks highly benefits from teacher supervision.
3. The supervised scheme is robust versus various kinds of noise affecting the synaptic tensor. This *ultra-noise tolerance* is achieved in the low load regime, where the redundancy of information in the couplings succeeds to mitigate the noise (see also [3] to deepen the role of redundancy in lowering the signal-to-noise threshold for pattern's detection).

As far as the computational and mathematical technicalities are concerned, even in supervised regime, the post-synaptic potentials do not share any Gaussian shape, thus universality of the quenched noise in spin glasses does not apply and standard techniques such as the replica trick and interpolation approaches do not work straightforwardly. We adapted the latter by implementing estimates on these distributions with large deviation theory and evaluated their averages by stability analysis, see appendix A: this route resulted in full accordance with numerical simulations.

Finally, we implemented a numerical Monte Carlo scheme that employs Plefka's effective dynamics to avoid any additional numerical slowdown related to the evaluation of the (huge) synaptic tensors (whose sizes get bigger as  $P$  grows) appearing in the dense scenario. It is worth noting that these technical extensions are of broad generality and can be applied to several other neural networks.

Beyond full coherence among analytical predictions and numerical simulations in the random setting, we also tested the whole theory on MNist and Fashion MNist datasets to observe that

- When the network lies in the retrieval region of its phase diagram, a single step of Plefka dynamics is sufficient to accomplish the classification task. This further corroborates the fact that classification with our networks is computationally inexpensive and highlights a practical usage of the knowledge stemming from the phase diagram
- The higher the interaction degree  $P$ , the higher the performance of the machine, being measured by classification accuracy, until a plateau is reached. This highlights the advantage of using networks characterized by higher-order interactions, especially equipped with supervised training as in this case the minimal dataset size for secure learning does not scale with  $P$ .

We conclude by pointing out that, despite working at the replica symmetric level of description, statistical mechanics techniques have made it possible to successfully employ a neural network at work with a classical computer vision task as image classification, suggesting that such a discipline can contribute to theoretical Artificial Intelligence by providing models and algorithms that can be fully understood both analytically and numerically -still accomplishing computational tasks of practical interest- and this can be particularly welcome in eXplainable AI (XAI); further, by the knowledge of the phase diagram, we can set the machine in optimal working regions (in the space of the control parameters) and this can be particularly welcome at work with optimization of algorithms and protocols, i.e., in the field of Sustainable AI (SAI).

## A Large Deviations Theory's computation

The purpose of this section is to show the goodness of the Gaussian approximation in Eq. (3.3). To do so, we use large deviations theory which helps us to understand the behaviour of tails in our distribution.

The random variable taken in consideration is

$$\sqrt{\frac{\beta'}{N^{P-1}\mathcal{R}^{P/2}}} \sum_{\mu>1}^K \sum_{i_1, \dots, i_{P/2}}^{N, \dots, N} \left( \frac{1}{M^{P/2}} \sum_{a_1, \dots, a_{P/2}}^{M, \dots, M} \xi_{i_1}^\mu \chi_{i_1}^{\mu, a_1} \dots \xi_{i_{P/2}}^\mu \chi_{i_{P/2}}^{\mu, a_{P/2}} \right) \sigma_{i_1} \dots \sigma_{i_{P/2}} z_\mu. \quad (\text{A.1})$$

If we consider  $\frac{1}{M} \sum_{a=1}^M \xi_i^\mu \chi_i^{\mu, a}$  we can apply CLT and approximate it as  $\frac{1}{M} \sum_{a=1}^M \xi_i^\mu \chi_i^{\mu, a} = \sqrt{\mathcal{R}} \lambda_i^\mu$  where  $\lambda_i^\mu \sim \mathcal{N}(0, 1)$ . Thus, reinserting in (A.1), we get

$$\sqrt{\frac{\beta'}{N^{P-1}}} \sum_{\mu>1}^K \sum_{i_1, \dots, i_{P/2}}^{N, \dots, N} \left( \lambda_{i_1}^\mu \dots \lambda_{i_{P/2}}^\mu \right) \sigma_{i_1} \dots \sigma_{i_{P/2}} z_\mu. \quad (\text{A.2})$$

If we retrieve  $\xi^1$ , we write (A.2) as

$$\sqrt{\beta' N} \sum_{\mu>1}^K \left( \frac{1}{N} \sum_i^N \lambda_i^\mu \xi_i^1 \right)^{P/2} z_\mu \quad (\text{A.3})$$

Now we work with fixed  $\mu$  and we focus only on  $\left( \frac{1}{N} \sum_i^N \lambda_i^\mu \xi_i^1 \right)^{P/2}$ . The addends in the sum w.r.t.  $i$  are altogether a Gaussian variable  $\mathcal{N}(0, 1)$ , since it is a product of a Gaussian with zero mean and a Rademacher variable. Thus, rather than keep  $\lambda_i^\mu \xi_i^1$  we can write only  $\lambda_i$ , where  $\lambda_i$  is a Gaussian variable ( $\mathcal{N}(0, 1)$ ). We now defined  $v$  as

$$v := \left( \frac{1}{N} \sum_i^N \lambda_i \right)^{P/2} \quad (\text{A.4})$$

We stress that the sum of Gaussian variable has again a normal distribution. However,  $v$  is  $P/2$ -th power of Gaussians, so we cannot say *a priori* that it can be considered as a normal variable.

Defining the generating function of moments for  $b := \frac{1}{N} \sum_{i=1}^N \lambda_i^a$  as

$$\phi(t) = \frac{1}{N} \log \mathbb{E} \exp(Ntb), \quad (\text{A.5})$$

we can compute the large deviations function through Legendre transformation:

$$l(b) = \max_t [\phi(t) - bt]. \quad (\text{A.6})$$

In our case we have

$$\phi(t) = \frac{t^2}{2} \quad (\text{A.7})$$

and  $l(b)$  is maximise when  $t = b$ ; reporting the value of  $t$  in  $l(b)$  we have

$$l(b) = -\frac{b^2}{2}. \quad (\text{A.8})$$

To sum up, the asymptotic distribution for the random variable  $b$  is

$$d\mathcal{P} = \frac{1}{\mathcal{Z}} \exp \left[ -\frac{N}{2} b^2 \right] db. \quad (\text{A.9})$$

where  $\mathcal{Z}$  is the partition function. Now, replacing  $b$  with  $v^{2/P}$  we have

$$d\mathcal{P} = \frac{1}{\mathcal{Z}} \exp \left[ -\frac{N}{2} v^{4/P} - \left(1 - \frac{2}{P}\right) \log v \right] dv \quad (\text{A.10})$$

As last step we compute the first and second momenta for  $v$  which are

$$(N)^{P/4} \langle |v| \rangle = \frac{2^{P/4} \Gamma \left( \frac{P+2}{4} \right)}{\sqrt{\pi}}, \quad (\text{A.11})$$

$$(N)^{P/2} \langle v^2 \rangle = \frac{2^{P/2} \Gamma \left( \frac{P+1}{2} \right)}{\sqrt{\pi}}. \quad (\text{A.12})$$

In the end, for  $P = 2$  and large values of  $N$  we have exactly a Gaussian distribution, as expected since  $v$  reduces to  $N^{-1} \sum_{i=1}^N \lambda_i$ . This is not true for  $P > 2$ ; however, since we have to sum an extensive number of variable  $v$  (we stress that at the beginning of our discussion we set  $\mu$  which is index of sum instead) and we can apply the Central Limit Theorem. Therefore, we can approximate our distribution to another one with suitable first and second momenta, for instance a Gaussian one.

## B Proof of Proposition 1

In order to prove Proposition 1 we need to introduce one more observable, linked to the additional set of real variables introduced through Hubbard-Stratonovich transformation:

$$p_{ab} := \frac{1}{K} \sum_{\mu=1}^K z_{\mu}^{(a)} z_{\mu}^{(b)}. \quad (\text{B.1})$$

where  $a, b$  are two replicas. Moreover, we state that, under the replica-symmetry assumption, in the thermodynamic limit, also this variable self-average under their mean values, i.e.

$$\lim_{N \rightarrow \infty} \langle (p_{12} - \bar{p})^2 \rangle_t = 0 \Rightarrow \lim_{N \rightarrow \infty} \langle p_{12} \rangle_t = \bar{p}. \quad (\text{B.2})$$

In order to prove the aforementioned proposition, we put in front of it the following

**Lemma 1.** *The  $t$  derivative of interpolating pressure is given by*

$$\begin{aligned} \frac{d\mathcal{A}_{N,K,\rho,\beta,r}^{(P)}}{dt} &= \frac{\beta'}{2} (1 + \rho)^{P/2} \langle n^P \rangle_t - \frac{\psi}{2} \langle n \rangle_t + \frac{\beta' \mathcal{V} K}{2 N^{P/2}} \left( \langle p_{11} \rangle_t - \langle q_{12}^{P/2} p_{12} \rangle_t \right) \\ &\quad - \frac{A^2}{2} (1 - \langle q_{12} \rangle_t) - \frac{B^2}{2} \frac{K}{N} (\langle p_{11} \rangle_t - \langle p_{12} \rangle_t) - \frac{C}{2} \frac{K}{N} \langle p_{11} \rangle_t. \end{aligned} \quad (\text{B.3})$$

Since the computation is lengthy but not cumbersome we decided to omit it.

**Assumption 1.** *For the generic order parameter  $X$  this can be rewritten as  $\langle (\Delta X)^2 \rangle \xrightarrow{N \rightarrow \infty} 0$ , where*

$$\Delta X := X - \bar{X},$$

*and, clearly, the RS approximation also implies that, in the thermodynamic limit,  $\langle \Delta X \Delta Y \rangle_t = 0$  for any generic pair of order parameters  $X, Y$ . Moreover in the thermodynamic limit, we have  $\langle (\Delta X)^k \rangle_t \rightarrow 0$  for  $k \geq 2$ .*

*From now on, we omit the subindex  $t$ .*

**Remark 4.** We stress that afterwards we use the relations

$$\begin{aligned}\langle n_1^P \rangle &= P \bar{n}^{P-1} \langle n_1 \rangle + \sum_{k=2}^P \binom{P}{k} \langle (n_1 - \bar{n})^k \rangle \bar{n}^{P-k} + (1 - P) \bar{n}^P, \\ \langle p_{12} q_{12}^{P/2} \rangle &= \bar{q}^{P/2} \langle p_{12} \rangle + \frac{P}{2} \bar{p} \bar{q}^{P/2-1} \langle q_{12} \rangle - \frac{P}{2} \bar{p} \bar{q}^{P/2} \\ &+ \sum_{k=1}^{P/2} \binom{\frac{P}{2}}{k} \bar{q}^{P/2-k} \langle (p_{12} - \bar{p})(q_{12} - \bar{q})^k \rangle + \sum_{k=2}^{P/2} \binom{\frac{P}{2}}{k} \bar{q}^{P/2-k} \bar{p} \langle (q_{12} - \bar{q})^k \rangle.\end{aligned}\tag{B.4}$$

which are computed with brute force with Newton's Binomial.

Now, using these relations, if we fix the four constants as

$$\begin{aligned}\psi &= P \beta' (1 + \rho)^{P/2} \bar{n}^{P-1} & A^2 &= \beta' \mathcal{V} K \frac{P}{2N^{P/2}} \bar{p} \bar{q}^{P/2-1} \\ B^2 &= \beta' \mathcal{V} N^{1-P/2} \bar{q}^{P/2} & C &= \beta' \mathcal{V} N^{1-P/2} (1 - \bar{q}^{P/2})\end{aligned}\tag{B.5}$$

we get the expression of derivative w.r.t.  $t$  reads as

$$\begin{aligned}\frac{d\mathcal{A}_{N,K,\rho,\beta,r}^{(P)}}{dt} &= \frac{\beta'}{2} (1 + \rho)^{P/2} (1 - P) \bar{n}^P - \beta' \mathcal{V} K \frac{P}{4N^{P/2}} \bar{p} \bar{q}^{P/2-1} (1 - \bar{q}) + \frac{\beta'}{2} (1 + \rho)^{P/2} \sum_{k=2}^P \binom{P}{k} \langle (n_1 - \bar{n})^k \rangle_t \bar{n}^{P-k} \\ &- \frac{\beta' \mathcal{V} K}{2} N^{-P/2} \left( \sum_{k=1}^{P/2} \binom{\frac{P}{2}}{k} \bar{q}^{P/2-k} \langle (p_{12} - \bar{p})(q_{12} - \bar{q})^k \rangle_t + \sum_{k=2}^{P/2} \binom{\frac{P}{2}}{k} \bar{q}^{P/2-k} \bar{p} \langle (q_{12} - \bar{q})^k \rangle_t \right)\end{aligned}\tag{B.6}$$

We stress that, due to RS assumption, in the thermodynamic limit, the potential  $V_N$  vanishes and the derivative w.r.t.  $t$  become

$$\frac{d\mathcal{A}_{N,K,\rho,\beta,r}^{(P)}}{dt} = \frac{\beta'}{2} (1 + \rho)^{P/2} (1 - P) \bar{n}^P - \beta' \mathcal{V} \alpha_b N^{b-P/2} \frac{P}{4} \bar{p} \bar{q}^{P/2-1} (1 - \bar{q}).\tag{B.7}$$

*Proof.* Let us start from finite size  $N$  expression. We apply the Fundamental Theorem of Calculus:

$$\mathcal{A}_{N,K,\rho,\beta,r}^{(P)} = \mathcal{A}_{N,K,\rho,\beta,r}^{(P)}(t=1) = \mathcal{A}_{N,K,\rho,\beta,r}^{(P)}(t=0) + \int_0^1 \partial_s \mathcal{A}_{N,K,\rho,\beta,r}^{(P)}(s) \Big|_{s=t} dt.\tag{B.8}$$

We have already computed the derivative w.r.t.  $t$  in Eq. (B.6). It only remains to calculate the one-body term:

$$\mathcal{Z}_{N,K,\rho,\beta,r}(t=0) = \sum_{\{\sigma\}} \exp \left[ \sum_{i=1}^N \left( \frac{\psi}{2} \frac{r}{\mathcal{R}} \hat{\chi}_M + A J_i \right) \sigma_i \right] \prod_{\mu>2}^K \int \frac{dz_\mu}{\sqrt{2\pi}} \exp \left[ \frac{1-C}{2} z_\mu^2 + B \tilde{J} z_\mu \right].\tag{B.9}$$

Using the definition of quenched statistical pressure (3.6) we have

$$\begin{aligned}\mathcal{A}_{N,K,\rho,\beta,r}^{(P)}(J, t=0) &= \ln \left[ 2 \cosh \left( \frac{\psi}{2} \frac{r}{\mathcal{R}} \hat{\chi}_M + A J_i \right) \right] - \frac{K}{2N} \ln (1 - C) + \frac{K}{2N} \frac{B^2}{1 - C} \\ &= \mathbb{E} \left\{ \ln 2 \cosh \left[ \beta' \frac{P}{2} \frac{(1 + \rho)^{P/2-1}}{r} \bar{n}^{P-1} \hat{\chi}_M + J \sqrt{\beta' \mathcal{V} \frac{KP}{2N^{P/2}} \bar{p} \bar{q}^{P/2-1}} \right] \right\} - \frac{\beta' \mathcal{V} K}{2N^{P/2}} \\ &- \frac{K}{2N} \ln \left[ 1 - \beta' \mathcal{V} N^{1-P/2} (1 - \bar{q}^{P/2}) \right] + \frac{\beta' \mathcal{V} K}{2N^{P/2}} \frac{\bar{q}^{P/2}}{1 - \beta' \mathcal{V} N^{1-P/2} (1 - \bar{q}^{P/2})} + V_N(t=0)\end{aligned}\tag{B.10}$$

where  $\mathbb{E} = \mathbb{E}_Y \mathbb{E}_\chi$  and

$$V_N(t) = \frac{\beta'}{2} (1 + \rho)^{P/2} \sum_{k=2}^P \binom{P}{k} \langle (n_1 - \bar{n})^k \rangle_t \bar{n}^{P-k} - \frac{\beta' \mathcal{V} K}{2} N^{-P/2} \left( \sum_{k=1}^{P/2} \binom{\frac{P}{2}}{k} \bar{q}^{P/2-k} \langle (p_{12} - \bar{p})(q_{12} - \bar{q})^k \rangle_t + \sum_{k=2}^{P/2} \binom{\frac{P}{2}}{k} \bar{q}^{P/2-k} \bar{p} \langle (q_{12} - \bar{q})^k \rangle_t \right). \quad (\text{B.11})$$

Finally, putting inside (B.10) and (B.6) in (B.8) and rescaling  $N^{b-P/2} \bar{p}$  as  $\bar{p}$  we reach the following expression:

$$\begin{aligned} \mathcal{A}_{N,K,\rho,\beta,r}^{(P)} &= \mathbb{E} \left\{ \ln 2 \cosh \left[ \beta' \frac{P}{2} \frac{(1 + \rho)^{P/2-1}}{r} \bar{n}^{P-1} \hat{\chi}_M + J \sqrt{\beta' \mathcal{V} \frac{K}{N^b} \frac{P}{2} \bar{p} \bar{q}^{P/2-1}} \right] \right\} + \\ &- \frac{K}{2N} \ln [1 - \beta' \mathcal{V} N^{1-P/2} (1 - \bar{q}^{P/2})] + \frac{\beta' \mathcal{V} K}{2N^{P/2}} \frac{\bar{q}^{P/2}}{1 - \beta' \mathcal{V} N^{1-P/2} (1 - \bar{q}^{P/2})} \\ &+ \frac{\beta'}{2} (1 + \rho)^{P/2} (1 - P) \bar{n}^P - \beta' \mathcal{V} \frac{K}{N^b} \frac{P}{4} \bar{p} \bar{q}^{P/2-1} (1 - \bar{q}) - \frac{\beta' \mathcal{V} K}{2N^{P/2}} + \int_0^1 V_N(t) dt. \end{aligned} \quad (\text{B.12})$$

where  $\mathbb{E} = \mathbb{E}_\chi \mathbb{E}_Y$ ,  $\hat{\chi}_M = \frac{1}{M} \sum_{a=1}^M \chi_i^{1,a}$  and  $V_N(t)$  as defined in Eq. (B.11).

In the thermodynamic limit, the potential  $V_N$  vanishes, so the expression of derivative w.r.t.  $t$  become (B.7).

Moreover, we are in high-load regime, namely we use the expression of load in Equation 2.11 with  $b = P - 1$ .

Finally, considering (B.12) and expanding w.r.t.  $\frac{1}{N} \rightarrow 0$  we reach the thesis.  $\square$

**Corollary 1.** *For large datasets  $M \gg 1$  in the high-storage regime, the replica-symmetric self-consistency equations (3.13)-(3.14) can be expressed as*

$$\bar{m} = \mathbb{E} \left[ \tanh g(\alpha_{P-1}, \tilde{\beta}, Z) \right], \quad (\text{B.13})$$

$$\bar{q} = \mathbb{E} \left[ \tanh^2 g(\alpha_{P-1}, \tilde{\beta}, Z) \right], \quad (\text{B.14})$$

$$\bar{n} = (1 + \rho)^{-1} \bar{m} + \beta' \frac{P}{2} \rho (1 + \rho)^{P/2-2} (1 - \bar{q}) \bar{n}^{P-1}. \quad (\text{B.15})$$

where

$$g(\beta, Z, \bar{m}) = \tilde{\beta} \frac{P}{2} \bar{m}^{P-1} + Z \tilde{\beta} \mathcal{V} \sqrt{\rho \left( \frac{P}{2} \bar{m}^{P-1} \right)^2 + \alpha_{P-1} \frac{P}{2} (1 + \rho)^P \bar{q}^{P-1}} \quad (\text{B.16})$$

with  $\mathbb{E} = \mathbb{E}_Z$  and  $\beta' = \tilde{\beta} (1 + \rho)^{P/2}$ .

*Proof.* For large datasets, using the Central Limit Theorem we have

$$\hat{\chi}_M \sim r + \sqrt{\frac{1 - r^2}{M}} Z. \quad (\text{B.17})$$

where  $Z$  is a standard Gaussian variable  $Z \sim \mathcal{N}(0, 1)$ . Replacing Eq. (B.17) in the self-consistency equation for  $\bar{n}$ , namely Eq. (3.13), and applying Stein's lemma<sup>8</sup> in order to recover the expression for  $\bar{m}$  and  $\bar{q}$ , we get the large dataset equation for  $\bar{n}$ , i.e. Eq. (B.15).

We now replace this new expression for  $\bar{n}$  in the argument of the other two self consistencies. We will use the relation

$$\mathbb{E}_{\lambda, Y}[F(a + b\lambda + cY)] = \mathbb{E}_Z[F(a + Z\sqrt{b^2 + c^2})], \quad (\text{B.19})$$

where  $\lambda, Y, Z$  are i.i.d. Gaussian variables,  $F(a + b\lambda + cY) = \tanh(a + b\lambda + c)$  and we pose  $a = \beta \frac{P}{2} \bar{m}^{P-1} (1 + \rho)^{-P/2}$ ,  $b = \beta' \frac{P}{2} \bar{n}^{P-1} (1 + \rho)^{P/2}$  and  $c = \beta' \mathcal{V} \sqrt{\alpha_{P-1} \frac{P}{2} \bar{q}^{P-1}}$ . Doing so, we obtain

$$g(\alpha_{P-1}, \tilde{\beta}, Z) = \tilde{\beta} \frac{P}{2} \bar{m}^{P-1} + Z \tilde{\beta} \sqrt{\rho \left( \frac{P}{2} \bar{m}^{P-1} \right)^2 + \alpha_{P-1} \mathcal{V}^2 \frac{P}{2} (1 + \rho)^P \bar{q}^{P-1}}, \quad (\text{B.20})$$

here we posed  $\beta' = \tilde{\beta}(1 + \rho)^{P/2}$  and we also truncated<sup>9</sup>  $\bar{n} \sim \bar{m}(1 + \rho)^{-1}$ .  $\square$

**Corollary 2.** *The self consistency equations in the large dataset assumption and null-temperature limit are*

$$\bar{m} = \text{erf} \left[ \frac{P \bar{m}^{P-1}}{2 G} \right],$$

$$G = \sqrt{2 \left[ \rho \left( \frac{P}{2} \bar{m}^{P-1} \right)^2 + \alpha_{P-1} \mathcal{V}^2 \frac{P}{2} (1 + \rho)^P \right]}, \quad (\text{B.21})$$

$$\bar{q} = 1.$$

*Proof.* We follow the same path of the unsupervised case in [1]. We start by assuming finite the limit

$$\lim_{\beta \rightarrow \infty} \beta(1 - \bar{q}) = D \in \mathbb{R} \quad (\text{B.22})$$

and we stress that as  $\tilde{\beta} \rightarrow \infty$  we have  $\bar{q} \rightarrow 1$ . As a consequence, the following reparametrization is found to be useful,

$$\bar{q} = 1 - \frac{\delta q}{\beta} \quad \text{as} \quad \beta \rightarrow \infty. \quad (\text{B.23})$$

We introduce the additional term  $\beta x$  in the argument of the hyperbolic tangent  $(g(\beta, Z, \bar{m}))$ , thus

$$\frac{\partial \bar{m}}{\partial x} = \beta \left[ 1 - \left( 1 - \frac{\delta \bar{q}}{\beta} \right) \right] = \delta \bar{q}. \quad (\text{B.24})$$

---

<sup>8</sup>This lemma, also known as Wick's theorem, applies to standard Gaussian variables, say  $J \sim \mathcal{N}(0, 1)$ , and states that, for a generic function  $f(J)$  for which the two expectations  $\mathbb{E}(Jf(J))$  and  $\mathbb{E}(\partial_J f(J))$  both exist, then

$$\mathbb{E}(Jf(J)) = \mathbb{E} \left( \frac{\partial f(J)}{\partial J} \right). \quad (\text{B.18})$$

<sup>9</sup>We notice that the second term right-side in (B.13), as far as the retrieval zone concerns,  $1 - \bar{q}$  has small value, and  $P$  is an even integer greater than 2.

Therefore, as  $\tilde{\beta} \rightarrow \infty$  and  $x \rightarrow 0$ , it yields

$$\bar{m} = \left\langle \text{sign} \left[ \frac{P}{2} \bar{m}^{P-1} + Z \sqrt{\rho \left( \frac{P}{2} \bar{m}^{P-1} \right)^2 + \alpha_{P-1} \mathcal{V}^2 \frac{P}{2} (1+\rho)^P} \right] \right\rangle_Z, \quad (\text{B.25})$$

$$\bar{q} \rightarrow 1 ;$$

to reach this result, we have also used the relation

$$\mathbb{E}_z \text{sign}[A + Bz] = \text{erf} \left[ \frac{A}{\sqrt{2}B} \right], \quad (\text{B.26})$$

where  $Z$  is a Gaussian variable  $\mathcal{N}(0, 1)$ ,  $A = \frac{P}{2} \bar{m}^{P-1}$  and  $B = \sqrt{\rho \left( \frac{P}{2} \bar{m}^{P-1} \right)^2 + \alpha_{P-1} \mathcal{V}^2 \frac{P}{2} (1+\rho)^P}$ .  $\square$

## C Evaluation of momenta of the effective post-synaptic potential

In this section we want to describe the computation of first and second momenta  $\mu_1$  and  $\mu_2$  in Sec. 4.1.

Let us start from  $\mu_1$ :

$$\mu_1 := \mathbb{E}_\xi \mathbb{E}_\chi \left[ \xi_i^1 h_i^{(1)}(\xi^1) \right] = \frac{\beta}{N^{P-1} M^P \mathcal{R}^{P/2}} \sum_{i_2, \dots, i_P}^{N, \dots, N} \sum_{a_1, \dots, a_P}^{M, \dots, M} \mathbb{E}_\chi \left[ \chi_{i_1}^{1, a_1} \dots \chi_{i_P}^{1, a_P} \right];$$

since  $\mathbb{E}_\xi[\xi_i^\mu] = 0$  the only non-zero terms are the ones with  $\mu = 1$ :

$$\begin{aligned} \mu_1 &:= \mathbb{E}_\xi \mathbb{E}_\chi \left[ \xi_i^1 h_i^{(1)}(\xi^1) \right] = \frac{\beta'}{2N^{P-1} M^P \mathcal{R}^{P/2}} \sum_{i_2, \dots, i_P}^{N, \dots, N} \sum_{a_1}^M \mathbb{E}_\chi \left[ \chi_{i_1}^{1, a_1} \right] \dots \sum_{a_P}^M \mathbb{E}_\chi \left[ \chi_{i_P}^{1, a_P} \right] \\ &= \frac{\beta'}{2N^{P-1} M^P \mathcal{R}^{P/2}} \sum_{i_2, \dots, i_P}^{N, \dots, N} M^P r^P = \frac{\beta'}{2} \left( \frac{r^2}{\mathcal{R}} \right)^{P/2} = \frac{\beta'}{2} (1+\rho)^{-P/2} \end{aligned} \quad (\text{C.1})$$

where we used  $\mathbb{E}_\chi[\chi_i^{\mu, a}] = r$ . Moving on, we start the computation of  $\mu_2$ :

$$\begin{aligned} \mu_2 &:= \mathbb{E}_\xi \mathbb{E}_\chi \left[ \{h_i^{(1)}(\xi^1)\}^2 \right] \\ &= \frac{\beta'^2}{4N^{2P-2} M^{2P} \mathcal{R}^P} \sum_{\mu, \nu=1}^K \sum_{a_1=1}^M \sum_{b_1=1}^M \sum_{\mathbf{a}, \mathbf{b}} \sum_{i_2, \dots, i_P}^M \sum_{j_2, \dots, j_P}^M \mathbb{E}_\chi \mathbb{E}_\xi \left[ \xi_{i_1}^\mu \xi_{i_1}^\nu \left( \xi_{i_2}^\mu \xi_{j_2}^\nu \dots \xi_{i_P}^\mu \xi_{j_P}^\nu \right) \left( \xi_{i_2}^1 \xi_{j_2}^1 \dots \xi_{i_P}^1 \xi_{j_P}^1 \right) \right. \\ &\quad \left. \chi_{i_1}^{\mu, a_1} \chi_{i_1}^{\nu, b_1} \left( \chi_{i_2}^{\mu, a_2} \chi_{j_2}^{\nu, b_2} \dots \chi_{i_P}^{\mu, a_P} \chi_{j_P}^{\nu, b_P} \right) \right] \end{aligned} \quad (\text{C.2})$$

Due to  $\mathbb{E}_\xi[\xi_{i_1}^\mu \xi_{i_1}^\nu] = \delta^{\mu\nu}$  the only non-zero terms are the ones with  $\mu = \nu$ :

$$\begin{aligned} \mu_2 &:= \mathbb{E}_\xi \mathbb{E}_\chi \left[ \{h_i^{(1)}(\xi^1)\}^2 \right] \\ &= \frac{\beta'^2}{4N^{2P-2} M^{2P} \mathcal{R}^P} \sum_{\mu=1}^K \sum_{a_1=1}^M \sum_{b_1=1}^M \sum_{\mathbf{a}, \mathbf{b}} \sum_{i_2, \dots, i_P}^M \sum_{j_2, \dots, j_P}^M \mathbb{E}_\chi \mathbb{E}_\xi \left[ \left( \xi_{i_2}^\mu \xi_{j_2}^\mu \dots \xi_{i_P}^\mu \xi_{j_P}^\mu \right) \left( \xi_{i_2}^1 \xi_{j_2}^1 \dots \xi_{i_P}^1 \xi_{j_P}^1 \right) \right. \\ &\quad \left. \chi_{i_1}^{\mu, a_1} \chi_{i_1}^{\mu, b_1} \left( \chi_{i_2}^{\mu, a_2} \chi_{j_2}^{\mu, b_2} \dots \chi_{i_P}^{\mu, a_P} \chi_{j_P}^{\mu, b_P} \right) \right] = A_{\mu=1} + B_{\mu>1} \end{aligned} \quad (\text{C.3})$$

namely we will analyze separately the case for  $\mu = 1$  ( $A_{\mu=1}$ ) and  $\mu > 1$  ( $B_{\mu>1}$ ).

$$\begin{aligned}
A_{\mu=1} &= \frac{\beta'^2}{4N^{2P-2}M^{2P}\mathcal{R}^P} \sum_{a_1=1}^M \sum_{b_1=1}^M \sum_{\mathbf{a}, \mathbf{b}} \sum_{i_2, \dots, i_P} \sum_{j_2, \dots, j_P} \mathbb{E}_\chi \left[ \chi_{i_1}^{1, a_1} \chi_{i_1}^{1, b_1} \left( \chi_{i_2}^{1, a_2} \chi_{j_2}^{1, b_2} \dots \chi_{i_P}^{1, a_P} \chi_{j_P}^{1, b_P} \right) \right] \\
&= \frac{\beta'^2}{4N^{2P-2}M^{2P}\mathcal{R}^P} \sum_{a_1=1}^M \sum_{\mathbf{a}, \mathbf{b}} \sum_{i_P} \sum_{j_2, \dots, j_P} \mathbb{E}_\chi \left[ \left( \chi_{i_2}^{1, a_2} \chi_{j_2}^{1, b_2} \dots \chi_{i_P}^{1, a_P} \chi_{j_P}^{1, b_P} \right) \right] \\
&\quad + \frac{\beta'^2}{4N^{2P-2}M^{2P}\mathcal{R}^P} \sum_{a_1=1}^M \sum_{b_1 \neq a_1} \sum_{\mathbf{a}, \mathbf{b}} \sum_{i_2, \dots, i_P} \sum_{j_2, \dots, j_P} \mathbb{E}_\chi \left[ \chi_{i_1}^{1, a_1} \chi_{i_1}^{1, b_1} \left( \chi_{i_2}^{1, a_2} \chi_{j_2}^{1, b_2} \dots \chi_{i_P}^{1, a_P} \chi_{j_P}^{1, b_P} \right) \right] \\
&= \frac{\beta'^2 r^{2P}}{4\mathcal{R}^P} \left( 1 + \frac{1-r^2}{Mr^2} \right) = \frac{\beta'^2}{4} (1+\rho)^{1-P}. \\
B_{\mu>1} &= \frac{\beta'^2}{4N^{2P-2}M^2} \sum_{\mu>1}^K \sum_{a_1=1}^M \sum_{b_1=1}^M \sum_{\mathbf{a}, \mathbf{b}} \sum_{i_2, \dots, i_P} \sum_{j_2, \dots, j_P} \mathbb{E}_\chi \mathbb{E}_\xi \left[ \left( \xi_{i_2}^\mu \xi_{j_2}^\mu \dots \xi_{i_P}^\mu \xi_{j_P}^\mu \right) \right. \\
&\quad \left. \left( \xi_{i_2}^1 \xi_{j_2}^1 \dots \xi_{i_P}^1 \xi_{j_P}^1 \right) \chi_{i_1}^{\mu, a_1} \chi_{i_1}^{\mu, b_1} \left( \chi_{i_2}^{\mu, a_2} \chi_{j_2}^{\mu, b_2} \dots \chi_{i_P}^{\mu, a_P} \chi_{j_P}^{\mu, b_P} \right) \right]
\end{aligned} \tag{C.4}$$

the only non-zero terms are the ones in which the sum over  $i$  and  $j$  will be equal in pairs:

$$\begin{aligned}
B_{\mu>1} &= \frac{\beta'^2}{4N^{2P-2}M^{2P}\mathcal{R}^P} (2P-3)!! \sum_{\mu>1}^K \sum_{\mathbf{a}, \mathbf{b}} \sum_{i_2, \dots, i_P} \mathbb{E}_\chi \left[ \chi_{i_1}^{\mu, a_1} \chi_{i_1}^{\mu, b_1} \left( \chi_{i_2}^{\mu, a_2} \chi_{i_2}^{\mu, b_2} \dots \chi_{i_P}^{\mu, a_P} \chi_{i_P}^{\mu, b_P} \right) \right] \\
&= \frac{\beta'^2}{4N^{2P-2}M^{2P}\mathcal{R}^P} (2P-3)!! \sum_{\mu>1}^K \sum_{i_2, \dots, i_P} \left( \sum_{a_1, b_1=1}^M \mathbb{E}_\chi \left[ \chi_{i_2}^{\mu, a_1} \chi_{i_2}^{\mu, b_1} \right] \dots \sum_{a_P, b_P=1}^M \mathbb{E}_\chi \left[ \chi_{i_P}^{\mu, a_P} \chi_{i_P}^{\mu, b_P} \right] \right)
\end{aligned} \tag{C.5}$$

To clarify the discussion, we now focus on

$$\begin{aligned}
\frac{1}{M^2} \sum_{a, b=1}^M \mathbb{E}_\chi \left[ \chi_i^{\mu, a} \chi_i^{\mu, b} \right] &= \frac{1}{M^2} \sum_{a=1}^M \mathbb{E}_\chi \left[ \chi_i^{\mu, a} \chi_i^{\mu, a} \right] + \sum_{a \neq b=1}^M \mathbb{E}_\chi \left[ \chi_i^{\mu, a} \chi_i^{\mu, b} \right] \\
&= \frac{1}{M^2} (M + M(M-1)r^2) = r^2 (1+\rho).
\end{aligned} \tag{C.6}$$

Inserting Eq. (C.6) in Eq. (C.5) we have

$$B_{\mu>1} = \frac{(\beta')^2(2P-3)!!}{4N^{P-1}\mathcal{R}^P} Kr^{2P} (1+\rho)^P = \frac{(\beta')^2(2P-3)!!}{4N^{P-1}} K; \tag{C.7}$$

if we set  $K = \alpha_{P-1} N^{P-1}$  we get

$$B_{\mu>1} = \frac{(\beta')^2(2P-3)!!}{4} \alpha_{P-1}. \tag{C.8}$$

Putting together Eq. (C.4) and Eq. (C.8) we reach the expression of  $\mu_2$ .

## D Plefka's Expansion on Gibbs potential

The purpose of this section is to follow the path from [49], namely the computation of the expansion of the Gibbs potential. We use this in the computational part of our work to produce the figures in

the main part. We remind to [1] for the discussion concerning dense Hebbian neural networks and dense unsupervised Hebbian networks. Let us describe the supervised regime.

The Hamiltonian of the described system is

$$\mathcal{H}_{N,K,r}^{(P)}(\boldsymbol{\sigma}|\boldsymbol{\xi}; z) = -\frac{1}{\sqrt{M^P \mathcal{R}^{P/2} P! N^{P-1}}} \sum_{\mu=1}^K \sum_{a_1, \dots, a_{P/2}=1}^M \sum_{i_1, i_2, \dots, i_{P/2}=1}^N \eta_{i_1}^{\mu, a_1} \dots \eta_{i_{P/2}}^{\mu, a_{P/2}} \sigma_{i_1} \dots \sigma_{i_{P/2}} z_\mu \quad (\text{D.1})$$

which is the interaction part of the integral representation of the Hamiltonian of dense Hebbian supervised network (3.1).

In order to proceed to our computations, we need to introduce a parameter  $\varphi$  and define an Hamiltonian  $H(\varphi)$  reads as

$$\mathcal{H}_{N,K,r}^{(P)}(\boldsymbol{\sigma}|\boldsymbol{\xi}; \mathbf{z}, \mathbf{h}, \tilde{\mathbf{h}}, \varphi) = \varphi \mathcal{H}_{N,K,r}^{(P)} - \frac{1}{\sqrt{M^P \mathcal{R}^{P/2} P! N^{P-1}}} \sum_i h_i \sigma_i - \sum_\mu \tilde{h}_\mu z_\mu; \quad (\text{D.2})$$

we stress that for  $\varphi = 0$  we have an Hamiltonian with non-interacting units, whereas for  $\varphi = 1$  we have one with full-interacting units;  $\{h_i\}$  and  $\{\tilde{h}_\mu\}$  are external fields which play a role on  $\boldsymbol{\sigma}$  and  $\mathbf{z}$  respectively.

Using (D.2) we write the partition function as

$$\begin{aligned} \mathcal{Z}_{\beta, N, K, r}^{(P)}(\varphi) &= \sum_{\boldsymbol{\sigma}} \int \prod_{\mu} dz_\mu \sqrt{\frac{\tilde{\beta}}{2\pi}} \exp \left( -\frac{\tilde{\beta}}{2} \sum_{\mu} z_\mu^2 \right. \\ &\quad - \frac{\varphi \tilde{\beta}}{\sqrt{M^P r^P N^{P-1}}} \sum_{\mu} \sum_{\mathbf{i}} \sum_{\mathbf{a}} \eta_{i_1}^{\mu, a_1} \dots \eta_{i_{P/2}}^{\mu, a_{P/2}} \sigma_{i_1} \dots \sigma_{i_{P/2}} z_\mu \\ &\quad \left. + \tilde{\beta} \sum_{\mu} \tilde{h}_\mu z_\mu + \frac{\tilde{\beta}}{\sqrt{M^P r^P N^{P-1}}} \sum_i h_i \sigma_i \right) \end{aligned} \quad (\text{D.3})$$

where  $\tilde{\beta}$  is defined as in Eq. (3.23).

Let us consider the Gibbs potential of this model, which is the Legendre transformation of the free energy constrained w.r.t. the magnetizations  $m_i = \langle \sigma_i \rangle$  and  $\langle z_\mu \rangle$  averaged w.r.t. Boltzmann distribution  $\propto \exp^{-\beta H(\varphi)}$ :

$$\mathcal{G}_{N,K,\beta,r}^{(P)}(\boldsymbol{\xi}; \mathbf{z}, \mathbf{h}, \tilde{\mathbf{h}}, \varphi) = -\frac{1}{\tilde{\beta}} \ln \mathcal{Z}_{\beta, N, K, r}^{(P)}(\varphi) + \sum_{\mu} \tilde{h}_\mu \langle z_\mu \rangle + \frac{1}{\sqrt{M^P r^P N^{P-1}}} \sum_i h_i m_i. \quad (\text{D.4})$$

Now we want to expand Gibbs potential around  $\varphi = 0$ , namely

$$\mathcal{G}_{N,K,\beta,r}^{(P)}(\boldsymbol{\xi}; \mathbf{z}, \mathbf{h}, \tilde{\mathbf{h}}, \varphi) = \mathcal{G}_{N,K,\beta,r}^{(P)}(\boldsymbol{\xi}; \mathbf{z}, \mathbf{h}, \tilde{\mathbf{h}}, \varphi = 0) + \sum_{n=1}^{\infty} \frac{\varphi^n \mathcal{G}^{(n)}}{n!} \quad \mathcal{G}^{(n)} = \left. \frac{\partial^n \mathcal{G}_{N,K,r}^{(P)}(\varphi)}{\partial \varphi^n} \right|_{\varphi=0}, \quad (\text{D.5})$$

and stop the expansion at the first order.

All we need is the non-interacting Gibbs potential  $\mathcal{G}_{N,K,\beta}^{(P)}(\boldsymbol{\xi}; \mathbf{z}, \mathbf{h}, \tilde{\mathbf{h}}, \varphi = 0)$  and the first derivative w.r.t.  $\varphi$ . Let us start from  $\mathcal{G}_{N,K,\beta}^{(P)}(\boldsymbol{\xi}; \mathbf{z}, \mathbf{h}, \tilde{\mathbf{h}}, \varphi = 0)$  (which from now is denoted  $\mathcal{G}(0)$ ).

$$\begin{aligned}\mathcal{G}(0) = & -\frac{N}{\tilde{\beta}} \log 2 - \frac{1}{\tilde{\beta}} \sum_i \log \cosh \left( \frac{\tilde{\beta}}{\sqrt{M^P r^P N^{P-1}}} h_i \right) + \sum_{\mu} \tilde{h}_{\mu} \langle z_{\mu} \rangle \\ & + \frac{1}{\sqrt{M^P r^P N^{P-1}}} \sum_i h_i \langle \sigma_i \rangle - \frac{1}{2} \sum_{\mu} \tilde{h}_{\mu}^2.\end{aligned}\quad (\text{D.6})$$

Now, if we extremize Eq. (D.6) w.r.t.  $h_i$  and  $\tilde{h}_{\mu}$  we find

$$h_i = \frac{\sqrt{M^P r^P N^{P-1}}}{\tilde{\beta}} \tanh^{-1}(m_i) \implies h_i = \frac{\sqrt{M^P r^P N^{P-1}}}{2\tilde{\beta}} \ln \left( \frac{1+m_i}{1-m_i} \right), \quad (\text{D.7})$$

$$\tilde{h}_{\mu} = \langle z_{\mu} \rangle. \quad (\text{D.8})$$

The last step is to insert the expressions (D.7) and (D.8) in the non-interacting Gibbs potential:

$$\begin{aligned}\mathcal{G}(0) = & -\frac{N}{\tilde{\beta}} \log 2 + \frac{1}{2\tilde{\beta}} \sum_i [(1-m_i) \log(1-m_i) + (1+m_i) \log(1+m_i)] \\ & + \frac{1}{2} \sum_{\mu} \langle z_{\mu} \rangle^2\end{aligned}\quad (\text{D.9})$$

Concerning the first order derivative w.r.t.  $\varphi$ , we have

$$\mathcal{G}^{(1)} = -\frac{1}{\sqrt{M^P r^P N^{P-1}}} \sum_{\mu} \sum_{i,a} \eta_{i_1}^{\mu,a_1} \dots \eta_{i_{P/2}}^{\mu,a_{P/2}} \langle z_{\mu} \rangle m_{i_1} \dots m_{i_{P/2}}. \quad (\text{D.10})$$

To sum up, we can write first order Gibbs potential (D.4) as

$$\begin{aligned}\mathcal{G}_{N,K,\beta}^{(P)}(\boldsymbol{\xi}; \boldsymbol{z}, \boldsymbol{h}, \tilde{\boldsymbol{h}}, \varphi) = & -\frac{N}{\tilde{\beta}} \log 2 + \frac{1}{2\tilde{\beta}} \sum_i [(1-m_i) \log(1-m_i) + (1+m_i) \log(1+m_i)] \\ & + \frac{1}{2} \sum_{\mu} \langle z_{\mu} \rangle^2 - \frac{\varphi}{\sqrt{N^{P-1}}} \sum_{\mu} \langle z_{\mu} \rangle \left( \frac{1}{rM} \sum_i \sum_a \eta_i^{\mu,a} m_i \right)^{P/2}\end{aligned}\quad (\text{D.11})$$

which allows us to compute the self-consistence equations for  $\varphi = 1$  as

$$m_i = \tanh \left\{ \tilde{\beta} \frac{P}{2} \frac{1}{\sqrt{N^{P-1}}} \sum_{\mu=1}^K \left[ \langle z_{\mu} \rangle \frac{1}{rM} \sum_{a=1}^M \eta_i^{\mu,a} \left( \frac{1}{rM} \sum_{b=1}^M \sum_{j=1}^N \eta_j^{\mu,b} m_j \right)^{P/2-1} \right] \right\}, \quad (\text{D.12})$$

$$\langle z_{\mu} \rangle = \frac{1}{\sqrt{N^{P-1}}} \left( \frac{1}{rM} \sum_{a=1}^M \sum_{i=1}^N \eta_i^{\mu,a} m_i \right)^{P/2}. \quad (\text{D.13})$$

In order to lighten the notation, we introduce the average of the examples reads as

$$\bar{\eta}_i^{\mu} = \frac{1}{M} \sum_{a=1}^M \eta_i^{\mu,a}, \quad (\text{D.14})$$

thus we can rewrite Eq. (D.12) and (D.13) as

$$m_i = \langle \sigma_i \rangle = \tanh \left\{ \tilde{\beta} \frac{P}{2} \frac{1}{\sqrt{N^{P-1}}} \sum_{\mu=1}^K \left[ \langle z_\mu \rangle \frac{1}{r} \bar{\eta}_i^\mu \left( \frac{1}{r} \sum_{j=1}^N \bar{\eta}_j^\mu m_j \right)^{P/2-1} \right] \right\}, \quad (\text{D.15})$$

$$\langle z_\mu \rangle = \frac{1}{\sqrt{N^{P-1}}} \left( \frac{1}{r} \sum_{i=1}^N \bar{\eta}_i^\mu m_i \right)^{P/2}. \quad (\text{D.16})$$

These equations are then used “in tandem” to make the system evolve: starting from an initial configuration  $\sigma^{(0)}$ , we evaluate the related  $z_\mu^{(0)}$  for any  $\mu$  and we use them in Eq. (D.15) to get  $m_i^{(0)}$  for any  $i$ , the latter is then used in Eq. (D.16) to get  $z_\mu^{(1)}$ , and we proceed this way, bouncing from (D.15) to (D.16), up to thermalization.

We stress that these equations allow to implement an effective dynamics that avoid the computation of spin configurations. In fact, this coarse grained dynamics only cares about the Boltzmann average of each spin direction, whose behaviour is given by Eq. (D.15). Even if at first glance Eq. (D.2) seems to require three set of auxiliary variables,  $\{z_\mu\}$ ,  $\{h_i\}$  and  $\{\tilde{h}_i\}$ , the extremization of the Gibbs potential at first order fixes the external fields  $\{h_i\}$  and  $\{\tilde{h}_i\}$ . The Gaussian variables  $\{z_\mu\}$  act as latent dynamical variables that evolve according to (D.16). In such an iterative MC scheme these hidden degrees of freedom are suitably updated in order to effectively retrieve the pattern that constitutes the signal.

As corroborating our results, we plot in Fig. 5 the results with MC simulations with Plefka’s dynamics and signal to noise analysis in terms of magnetization  $m$  and susceptibility  $\partial_r m$ . We show that they are perfectly aligned. Furthermore, in Fig. 6 we plot the attractors for a random pattern using MC simulations with Plefka’s dynamics. We highlight that, as  $\rho$  increases, the attractors shrinks.

## Table of symbols (in alphabetical order)

- $\mathcal{A}$  is the statistical quenched pressure
- $\alpha_b$  is the storage of the network defined as  $\alpha_P = \lim_{N \rightarrow +\infty} K/N^b$
- $\mathcal{B}(\sigma; t)$  is the Boltzmann factor, defined as  $\mathcal{B}(\sigma; t) = \exp[\beta H(\sigma; t)]$
- $\beta$  is a non negative constant called (fast) noise such that for  $\beta \rightarrow 0$  the behavior of the network is a pure random walk while for  $\beta \rightarrow \infty$  it is a steepest descent toward the minima
- $\mathbb{E}$  denotes the average over all the variables took in examination
- $\eta \in \{-1, +1\}^{K \times M}$  are the noisy examples, namely a noisy version of the archetypes, where  $\eta^{\mu, a} = \xi^\mu \chi^{\mu, a}$
- $\gamma$  is the  $P$  independent part of  $\alpha_b$ , namely  $\alpha_b = \gamma \frac{2}{P(2P-3)!!}$
- $H$  is the Hamiltonian of the model
- $K \in \mathbb{N}$  is the amount of archetypes  $\xi$  to learn and retrieve, in the maximum storage limit  $K = \gamma \frac{2}{P(2P-3)!!} N^{P-1}$
- $N \in \mathbb{N}$  is the amount of spins of the network, also known as network size
- $M \in \mathbb{N}$  is the amount of examples per archetype
- $m_\mu$  is the Mattis magnetization w.r.t. the archetype  $\xi^\mu$  defined as  $\frac{1}{N} \sum_i \xi_i^\mu \sigma_i$ . We always take into consideration  $m_1$ . In RS assumption the thermodynamic limit is  $\bar{m}$
- $n_\mu$  is the magnetization w.r.t. the example  $\eta^{\mu, a}$  defined as  $\frac{r}{\mathcal{R}NM} \sum_{i, a} \eta_i^{\mu, a} \sigma_i$ . In RS assumption the thermodynamic limit is  $\bar{n}_\mu$
- $\omega_t(O(\sigma))$  is the generalized Boltzmann measure, namely  $\omega_t(O(\sigma)) = \frac{1}{Z_N} \sum_{\sigma} O(\sigma) \mathcal{B}(\sigma; t)$
- $P$  is the degree of interaction among spins of the network
- $p$  is the probability of flipping w.r.t. the archetypes
- $p_{ab}$  is the overlap among the real gaussian variables  $z_\mu$  defined as  $\frac{1}{KM} \sum_\mu z_\mu^{(a)} z_\mu^{(b)}$ . In RS assumption the thermodynamic limit is  $\bar{p}$ .
- $q_{ab}$  is the overlap among two replicas, namely two identical copies of spin configurations which share quenched noise defined as  $\frac{1}{N} \sum_i \sigma_i^{(a)} \sigma_i^{(b)}$ . In RS assumption the thermodynamic limit is  $\bar{q}$
- $\mathcal{R}$  is defined as  $\mathcal{R} = r^2 + \frac{1-r^2}{M}$
- $r$  assesses the dataset quality such that  $p = \frac{1-r}{2}$ ; for  $r \rightarrow 1$  the example matches perfectly with the archetype whereas for  $r = 0$  solely noise remains
- $\rho$  quantifies the ignorance of the archetypes dataset, namely  $\rho = \frac{1-r^2}{r^2 M}$
- $t$  is the parameter for Guerra's interpolation; when  $t = 1$  we recover the original model, whereas for  $t = 0$  we compute the one-body terms

- $\mathcal{V}$  is the right variance to be set a posteriori using the signal to noise analysis, namely  $\mathcal{V} = \sqrt{\frac{P(2P-3)!!}{2}}$
- $\mathcal{Z}$  is the partition function
- $\langle O(\sigma) \rangle$  is the generalize average defined as  $\langle O(\sigma) \rangle = \mathbb{E}\omega_t(O(\sigma))$

## Acknowledgments

This work is supported by Ministero degli Affari Esteri e della Cooperazione Internazionale (MAECI) via the BULBUL grant (Italy-Israel), CUP Project n. F85F21006230001.

E.A. acknowledges financial support from Sapienza University of Rome (RM120172B8066CB0).

D.L. acknowledges INdAM (Istituto Nazionale d'Alta Matematica) and C.N.R. (National Research Council), and A.A. acknowledges UniSalento, both for financial support via PhD-AI.

## References

- [1] E. Agliari, L. Albanese, F. Alemanno, A. Alessandrelli, A. Barra, F. Giannotti, D. Lotito, and D. Pedreschi. Dense Hebbian neural networks: a replica symmetric picture of unsupervised learning. *preprint arXiv*, 2022.
- [2] E. Agliari, L. Albanese, F. Alemanno, and A. Fachechi. A transport equation approach for deep neural networks with quenched random weights. *Journal of Physics A: Mathematical and Theoretical*, 54, 2021.
- [3] E. Agliari, F. Alemanno, A. Barra, M. Centonze, and A. Fachechi. Neural networks with a redundant representation: Detecting the undetectable. *Physical Review Letters*, 124:28301, 2020.
- [4] E. Agliari, F. Alemanno, A. Barra, and A. Fachechi. Generalized guerra's interpolation schemes for dense associative neural networks. *Neural Networks*, 128:254–267, 2020.
- [5] E. Agliari, F. Alemanno, A. Barra, and G. D. Marzo. The emergence of a concept in shallow neural networks. *Neural Networks*, 148:232–253, 2022.
- [6] E. Agliari, A. Barra, R. Burioni, and A. D. Biasio. Notes on the p-spin glass studied via hamilton-jacobi and smooth-cavity techniques. *Journal of Mathematical Physics*, 53:1–36, 2012.
- [7] E. Agliari, A. Barra, P. Sollich, and L. Zdeborová. Machine learning and statistical physics: preface, 2020.
- [8] E. Agliari and G. D. Marzo. Tolerance versus synaptic noise in dense associative memories. *European Physical Journal Plus*, 135, 2020.
- [9] L. Albanese, F. Alemanno, A. Alessandrelli, and A. Barra. Replica symmetry breaking in dense hebbian neural networks. *J. Stat. Phys.*, 189(2):1–41, 2022.
- [10] L. Albanese, F. Alemanno, A. Alessandrelli, and A. Barra. Replica symmetry breaking in dense hebbian neural networks. *J. Stat. Phys.*, 189(2):1–41, 2022.
- [11] D. Alberici, A. Barra, P. Contucci, and E. Mingione. Annealing and replica-symmetry in deep boltzmann machines. *Journal of Statistical Physics*, 180(1):665–677, 2020.
- [12] F. Alemanno, M. Aquaro, I. Kanter, A. Barra, and E. Agliari. Supervised hebbian learning. *Europhysics Letters*, *in press*, 2022.
- [13] D. J. Amit. *Modeling brain function: The world of attractor neural networks*. Cambridge university press, 1989.

- [14] D. J. Amit, H. Gutfreund, and H. Sompolinsky. Storing infinite numbers of patterns in a spin-glass model of neural networks. *Physical Review Letters*, 55:1530–1533, 1985.
- [15] A. Auffinger and A. Jagannath. Thouless–anderson–palmer equations for generic p-spin glasses. *The Annals of Probability*, 47(4):2230, 2019.
- [16] A. Auffinger and Z. Qiang. Existence of two-step replica symmetry breaking for the spherical mixed p-spin glass at zero temperature. *Nature*, 370:377, 2019.
- [17] Y. Bahri, J. Kadmon, J. Pennington, S. S. Schoenholz, J. Sohl-Dickstein, and S. Ganguli. Statistical mechanics of deep learning. *Annual Review of Condensed Matter Physics*, 11:1, 2020.
- [18] P. Baldi and S. S. Venkatesh. Number of stable points for spin-glasses and neural networks of higher orders. *Physical Review Letters*, 58, 1987.
- [19] H. Bao, R. Zhang, and Y. Mao. The capacity of the dense associative memory networks. *Neurocomputing*, 469:198–208, 2022.
- [20] A. Barra, A. Bernacchia, E. Santucci, and P. Contucci. On the equivalence of Hopfield networks and Boltzmann Machines. *Neural Networks*, 34:1–9, 2012.
- [21] A. Barra, G. Genovese, and F. Guerra. The replica symmetric approximation of the analogical neural network. *Journal of Statistical Physics*, 140:784–796, 2010.
- [22] A. Barra, G. Genovese, F. Guerra, and D. Tantari. How glassy are neural networks? *Journal of Statistical Mechanics: Theory and Experiment*, 2012(07):P07009, 2012.
- [23] D. Belius and M. Schmidt. Phase diagram for the tap energy of the  $p$ -spin spherical mean field spin glass model. *arXiv preprint*, page 2207.02821, 2022.
- [24] A. Bovier and B. Niederhauser. The spin-glass phase-transition in the Hopfield model with p-spin interactions. *Advances in Theoretical and Mathematical Physics*, 5:1001–1046, 8 2001.
- [25] B. Bravi, P. Sollich, and M. Opper. Extended plefka expansion for stochastic dynamics. *Journal of Physics A: Mathematical and General*, 49, 2016.
- [26] T. Castellani and A. Cavagna. Spin-glass theory for pedestrians. *Journal of Statistical Mechanics*, 05:P05012, 2005.
- [27] A. C. C. Coolen, R. Kühn, and P. Sollich. *Theory of neural information processing systems*. OUP Oxford, 2005.
- [28] A. Decelle, F. Krzakala, C. Moore, and L. Zdeborova. Inference and phase transitions in the detection of modules in sparse networks. *Physical Review Letters*, 107(6):065701, 2011.
- [29] L. Deng. The mnist database of handwritten digit images for machine learning research. *IEEE Signal Processing Magazine*, 29(6):141–142, 2012.
- [30] A. Engel and C. Van den Broeck. *Statistical mechanics of learning*. Cambridge University Press, 2001.
- [31] E. Gardner. Multiconnected neural network models. *Journal of Physics A: Mathematical and General*, 20.11:3453, 1987.
- [32] E. J. Gardner, D. Wallace, and N. Stroud. Training with noise and the storage of correlated patterns in a neural network model. *Journal of Physics A: Mathematical and General*, 22(12):2019, 1989.
- [33] B. A. Gerard, E. Subag, and O. Zeitouni. Geometry and temperature chaos in mixed spherical spin glasses at low temperature: the perturbative regime. *Communications on Pure and Applied Mathematics*, 73:1732, 2020.
- [34] C. G. Gross. Genealogy of the “grandmother cell”. *The Neuroscientist*, 8.5:512, 2002.

[35] F. Guerra. Broken replica symmetry bounds in the mean field spin glass model. *Communications in Mathematical Physics*, 233:1–12, 2003.

[36] H. Huang. Mechanisms of dimensionality reduction and decorrelation in deep neural networks. *Physical Review E*, 98(6):062313, 2018.

[37] H. Huang. *Statistical Mechanics of Neural Networks*. Springer press, 2021.

[38] I. Kanter and H. Sompolinsky. Associative recall of memory without errors. *Physical Review A*, 35:1:380, 1987.

[39] D. Krotov and J. Hopfield. Dense associative memory is robust to adversarial inputs. *Neural Computation*, 30:3151–3167, 2018.

[40] D. Krotov and J. Hopfield. Large associative memory problem in neurobiology and machine learning. *arXiv*, page 2008.06996, 2020.

[41] D. Krotov and J. J. Hopfield. Dense associative memory for pattern recognition. *Advances in Neural Information Processing Systems*, pages 1180–1188, 2016.

[42] F. E. Leonelli, E. Agliari, L. Albanese, and A. Barra. On the effective initialisation for restricted boltzmann machines via duality with hopfield model. *Neural Networks*, 143:314–326, 2021.

[43] T. Lesieur, L. Miolane, M. Lelarge, F. Krzakala, and L. Zdeborova. Statistical and computational phase transitions in spiked tensor estimation. *IEEE International Symposium on Information Theory*, page 511, 2017.

[44] Y. Meir, S. Sardi, S. Hodassman, K. Kisos, I. Ben-Noam, A. Goldental, and I. Kanter. Power-law scaling to assist with key challenges in artificial intelligence. *Scientific Reports*, 10:1:1, 2020.

[45] M. Mézard, G. Parisi, and M. A. Virasoro. *Spin glass theory and beyond: an introduction to the Replica Method and its applications*, volume 9. World Scientific Publishing Company, 1987.

[46] M. Mezard, G. Parisi, and R. Zecchina. Analytic and algorithmic solution of random satisfiability problems. *Science*, 297(5582):812, 2002.

[47] M. Pankaj and D. J. Schwab. An exact mapping between the variational renormalization group and deep learning. *arXiv preprint*, 1410.3831, 2014.

[48] M. Pastore, A. Di Gioacchino, and P. Rotondo. Large deviations of the free energy in the p-spin glass spherical model. *Physical Review Research*, 1(3):033116, 2019.

[49] T. Plefka. Convergence condition of the TAP equation for the infinite-ranged Ising spin glass model. *Journal of Physics A: Mathematical and General*, 15, 1982.

[50] T. J. Sejnowski. Higher-order boltzmann machines. In *AIP Conference Proceedings*, volume 151, 1, pages 398–403. American Institute of Physics, 1986.

[51] H. Seung, H. Sompolinsky, and N. Tishby. Statistical mechanics of learning from examples. *Physical review A*, 45(8):1992, 6056.

[52] E. Subag and O. Zeitouni. Concentration of the complexity of spherical pure p-spin models at arbitrary energies. *Nature*, 62:123301, 2021.

[53] H. Uzan, S. Sardi, A. Goldental, R. Vardi, and I. Kanter. Biological learning curves outperform existing ones in artificial intelligence algorithms. *Scientific Reports*, 9:11:1, 2019.

[54] M. Welling and G. Hinton. A new learning algorithm for mean field Boltzmann machines. *International Conference on Artificial Neural Networks*, 8(5):351, 2002.

[55] M. Wong and D. Sherrington. Neural networks optimally trained with noisy data. *Physical Review E*, 47(6):1993, 4465.

[56] H. Xiao, K. Rasul, and R. Vollgraf. Fashion-MNIST: a Novel Image Dataset for Benchmarking Machine Learning Algorithms. *arXiv preprint arXiv:1708.07747*, pages 1–6, 2017.